Oxygen control of breathing by an olfactory receptor activated by lactate

Andy J. Chang[1], **Fabian E. Ortega**[1], **Johannes Riegler**[2,†], **Daniel V. Madison**[3], and **Mark A. Krasnow**[1]

[1]Department of Biochemistry, Stanford University School of Medicine and Howard Hughes Medical Institute, Stanford, California 94305, USA.

[2]Department of Medicine, Stanford University School of Medicine, Stanford, California 94305, USA.

[3]Department of Molecular and Cellular Physiology, Stanford University School of Medicine, Stanford, California 94305, USA.

Summary

Animals have evolved homeostatic responses to changes in oxygen availability that act on different time scales. Although the hypoxia-inducible factor (HIF) transcriptional pathway that controls long term responses to low oxygen (hypoxia) has been established[1], the pathway that mediates acute responses to hypoxia in mammals is not well understood. Here we show that the olfactory receptor *Olfr78* is highly and selectively expressed in oxygen-sensitive glomus cells of the carotid body, a chemosensory organ at the carotid artery bifurcation that monitors blood oxygen and stimulates breathing within seconds when oxygen declines[2]. *Olfr78* mutants fail to increase ventilation in hypoxia but respond normally to hypercapnia. Glomus cells are present in normal numbers and appear structurally intact, but hypoxia-induced carotid body activity is diminished. Lactate, a metabolite that rapidly accumulates in hypoxia and induces hyperventilation[3–6], activates Olfr78 in heterologous expression experiments, induces calcium transients in glomus cells, and stimulates carotid sinus nerve activity through Olfr78. We propose that in addition to its role in olfaction, Olfr78 acts as a hypoxia sensor in the breathing circuit by sensing lactate produced when oxygen levels decline.

The carotid body is the major sensor of blood oxygen in mammals. It is stimulated by a reduction in arterial blood oxygen from 100 mmHg to <80 mmHg. A current model is that hypoxia causes closure of K^+ channels of glomus cells, stimulating Ca^{+2}-dependent release of neurotransmitters onto afferent nerves that signal to brainstem respiratory centers. However, the oxygen sensor and sensing mechanism that trigger these events in glomus cells remain controversial[2] (Extended Data Fig. 1a–d). To identify new candidate molecules involved in carotid body oxygen sensing, we used RNA sequencing and whole genome microarrays to compare gene expression of the carotid body from wild-type adult C57BL/6J mice to that of the adrenal medulla, which shares developmental and functional similarities with the carotid body but does not respond acutely to hypoxia[7]. We reasoned that an oxygen sensor would be expressed at high levels in carotid body relative to adrenal medulla, and focused on signaling molecules that can act on the acute time scale of carotid body sensing. Transcripts for the olfactory receptor *Olfr78* were highly expressed in carotid body (top 4% of all genes by RNA sequencing) and highly enriched relative to adrenal medulla by both RNA sequencing (92-fold) and microarrays (3 probe sets, 17 to 80-fold) (Fig. 1a, b, Extended Data Fig. 2a–d, and Extended Data Table 1).

Olfactory receptors (ORs) comprise a subfamily of G protein-coupled receptors that is the largest gene family in vertebrates, encoded by ~1,200 genes in mouse[8]. ORs are expressed in olfactory sensory neurons and detect volatile odorants in smell. However, some ORs are expressed in other tissues[8–10]. The RNA sequencing results showed that three other OR genes (*Olfr1033, Olfr613*, and *Olfr856ps1*) were expressed (RPKM>2) in the carotid body, but at similar levels in adrenal medulla and thus not pursued further (Fig. 1b and Extended Data Fig. 2b). *Olfr558* was highly and selectively expressed in the carotid body, but at lower levels than *Olfr78* (Fig. 1a, b). *Olfr78* and *Olfr558* encode closely related proteins of the same OR subfamily and lie in close proximity in the genome (Extended Data Fig. 2e). Because of the high and selective expression of *Olfr78* and *Olfr558* in the carotid body, we investigated their expression and potential function.

The carotid body is composed of Type I glomus cells that sense changes in oxygen, Type II sustentacular cells that resemble neuroglia, nerve fibers, and endothelial and smooth muscle cells that comprise fine tortuous vessels off the carotid artery (Extended Data Fig. 1b). To determine which cells express *Olfr78*, we used an *Olfr78* reporter strain carrying *GFP* and *taulacZ* genes in the 3'-untranslated region (3'-UTR) of the *Olfr78* locus[11]. X-gal staining for lacZ activity in adults confirmed strong and selective *Olfr78* expression in carotid body and no detectable adrenal gland expression (Fig. 1c–f). The cluster-like pattern of X-gal staining in carotid body suggested *Olfr78* is expressed in glomus cells (Fig. 1d–f). This was verified by antibody staining showing co-localization of *Olfr78* reporter GFP with tyrosine hydroxylase (TH), a glomus cell marker (Fig. 1g, h); 98% of all GFP and TH-positive cells expressed both markers (*n*=3 sections from 3 animals, 222 cells). Unlike the monoallelic expression of olfactory receptors observed in olfactory neurons[12], we found that in animals carrying only one allele of the *Olfr78* reporter gene, 98% of all GFP and TH-positive cells still expressed both markers (*n*=3 sections from 3 animals, 271 cells, *P*=0.461 Tg/+ vs. Tg/Tg by unpaired *t* test) (Extended Data Fig. 3a). Using an *Olfr558 lacZ* knock-in reporter allele, we detected reporter activity in some vascular smooth muscle cells of carotid body

blood vessels, but not in glomus cells (Extended Data Fig. 3e–h). Thus we focused on *Olfr78*.

Although *Olfr78* and its human ortholog *OR51E2* are expressed in other tissues outside the olfactory system[9,10,13,14], no expression of *Olfr78* reporter was detected in other parts of the oxygen-sensing circuit for breathing besides carotid body (Extended Data Fig. 1c): carotid sinus and glossopharyngeal nerves (Fig. 1i–k), petrosal, nodose/jugular, and superior cervical ganglia (Fig. 1i–k and Extended Data Fig. 3b, c), and brainstem (Extended Data Fig. 3d). In some carotid bifurcations, there were patches of *Olfr78*-expressing cells on arteries that were innervated by branches of the glossopharyngeal nerve distinct from the carotid sinus nerve (Fig. 1j); these may be ectopic "miniglomera" with chemosensory functions similar to carotid body[15]. We conclude that *Olfr78* is specifically expressed in acute oxygen-sensing cells of the carotid body and not in afferent pathways or the respiratory centers themselves.

Because ORs mediate acute sensory signaling in olfaction, we tested whether Olfr78 was involved in acute oxygen sensing in the carotid body by examining breathing of *Olfr78* knockout mice[16]. Homozygous $Olfr78^{-/-}$ mutants were viable and present in Mendelian ratios at birth (postnatal day 1 (P1); 15 +/+:35 +/−:19 −/−, χ2=0.4783, *P*>0.7) and weaning (P21; 50 +/+:115 +/−:64 −/−, χ2=1.7162, *P*>0.3), and they appeared to breathe and behave normally under ambient conditions. However, when challenged by hypoxia (10% O_2), $Olfr78^{+/+}$ control animals increased respiratory rate and minute ventilation, whereas $Olfr78^{-/-}$ mutants did not exhibit significant ventilatory changes (Fig. 2a, b and Extended Data Fig 4a, b). Most strikingly, the respiratory rate of $Olfr78^{-/-}$ mutants did not change in hypoxia, while increasing ~30% in controls (Fig. 2a, b). In hypoxia, arterial blood from $Olfr78^{-/-}$ mutants had higher $PaCO_2$ and lower pH than wild-type animals (Extended Data Fig. 5a–f), consistent with their inability to increase ventilation. By contrast, ventilatory responses to hypercapnia (5% CO_2) remained intact in $Olfr78^{-/-}$ mutants (Fig. 2c, d and Extended Data Fig. 4c, d), as did two other rapid behavioral responses to hypoxia: reduced locomotion and more regular breathing (Supplementary Video 1). We also did not detect differences between controls and $Olfr78^{-/-}$ mutants in body temperature or metabolism in response to hypoxia (Extended Data Fig. 5g–j), parameters that can affect hypoxic ventilation in small mammals[17]. Thus, $Olfr78^{-/-}$ mutants have a specific defect in hypoxic regulation of respiratory rate, a physiological function controlled by the carotid body[2].

Previous studies showed that mice with fewer carotid body glomus cells have attenuated responses to hypoxia[18]. We examined developmental expression of *Olfr78* in carotid body and found it was not expressed embryonically, when transcription factors that regulate carotid body development are detected and glomus cells form[18]. *Olfr78* expression was first observed after birth before maturation of carotid body oxygen sensing, and persisted throughout adult life (Fig. 1l). The number of TH-positive glomus cells and their organization into clusters were not affected in $Olfr78^{-/-}$ mutants (Fig. 3a–c). We also did not detect ultrastructural defects: mutant glomus cells still contained the normal large dense core vesicles all along the plasma membrane and small clear core vesicles at synapses[2] (Fig. 3d–g). Thus, glomus cells are present in normal numbers and appear structurally intact in $Olfr78^{-/-}$ mutants.

To assess carotid body oxygen sensing, we carried out extracellular recordings of the carotid sinus nerve (Extended Data Fig. 1b, c), a standard assay of carotid body neurosensory activity. We found that carotid sinus nerves from *Olfr78*$^{-/-}$ mutants had similar baseline discharge frequencies as *Olfr78*$^{+/+}$ and *Olfr78*$^{+/-}$ controls, demonstrating that nerve activity is intact in *Olfr78*$^{-/-}$ mutants. However, in hypoxia (PO$_2$=60–80 mmHg), control nerve activity increased substantially whereas *Olfr78*$^{-/-}$ mutant nerve activity showed little response (Fig. 3h and Extended Data Fig. 6a–h). By contrast, carotid sinus nerve activation by low pH was intact in *Olfr78*$^{-/-}$ mutants (Fig. 3i and Extended Data Fig. 6i, j). We conclude that *Olfr78* mutants have a specific defect in carotid body oxygen sensing.

Previous studies demonstrating the robust response of carotid body and breathing to cyanide and other electron transport inhibitors suggest that carotid body oxygen sensing may be mediated by a sensor that detects changes in metabolism[2] (Extended Data Fig. 1d, e). Interestingly, two short-chain fatty acids, acetate and propionate, activate Olfr78 and its human ortholog OR51E2 expressed in HEK293T cells, with EC$_{50}$ values of 1–3 mM[14,19]. However, blood concentrations of acetate and propionate in rodents and humans are only 0.1–0.3 mM and 4–25 μM, respectively[20,21], and change little in hypoxia relative to the Olfr78 activation curve[22]. Thus, we sought a ligand for Olfr78 that is present in blood and tissue and effective at physiologically relevant levels.

One appealing candidate that is chemically similar to acetate and propionate but more abundant *in vivo* is lactate, which is found in blood and tissue at low mM concentrations and rapidly increases in hypoxia (Extended Data Fig. 1e). Using a heterologous expression assay, we found that lactate activated Olfr78 in a dose-dependent manner with an EC$_{50}$ of 4.0 mM (Fig. 4a and Extended Data Fig. 7a–g). Chloride ion over the same range of concentrations and osmolarity had no effect, whereas propionate and acetate stimulated Olfr78 with EC$_{50}$ values similar to previous findings[14] (Extended Data Fig. 7d–g). Because lactate concentrations in blood, tissue, and tissue interstitium are 1–5 mM (Extended Data Fig. 1e), the observed EC$_{50}$ value of 4.0 mM for Olfr78 renders it highly sensitive to small changes in lactate in the physiological range. Indeed, hypoxia and mitochondrial poisons such as cyanide elevate plasma and tissue lactate concentrations rapidly in this range (Extended Data Fig. 1e). We observed that arterial blood lactate increased from 3 mM to 6 mM within 3–5 minutes of hypoxia in both control and *Olfr78*$^{-/-}$ mutant animals (Fig. 4b and Extended Data Fig. 7h). Thus, lactate activates Olfr78 in a physiologically relevant range.

Mitochondrial poisons trigger carotid body glomus cell activity[23], and acute lactate application depolarizes glomus cells, stimulates carotid sinus nerve activity, and induces hyperventilation[3,4,24,25]. To determine if lactate can directly activate glomus cells, we carried out functional imaging experiments by expressing the calcium indicator GCaMP3 in glomus cells (Extended Data Fig. 8a–e). In both whole carotid bodies and slice preparations, we found that lactate induced calcium transients in glomus cells, as did hypoxia or addition of cyanide to inhibit mitochondrial electron transport chain and block oxygen consumption (Fig. 4c, d and Extended Data Fig. 8f–i). The response to lactate was stronger in slices than in intact carotid bodies, perhaps because glomus cells in slices have more direct exposure to lactate in the superperfusate (Fig. 4f). We conclude that lactate can acutely activate glomus

cells, much like hypoxia and cyanide. Interestingly, in both these experiments and carotid sinus nerve recordings (ref[25] and see below), carotid body activation by lactate was observed in hyperoxia, suggesting that lactate can stimulate carotid body sensory activity in the absence of other hypoxic signals.

To determine if carotid body activation by lactate requires Olfr78, we examined the effect of lactate on carotid sinus nerve activity in $Olfr78^{-/-}$ mutants. While lactate increased carotid sinus nerve activity in preparations from wild-type $Olfr78^{+/+}$ animals as expected[25], there was little response to lactate in $Olfr78^{-/-}$ mutant nerves (Fig. 4e and Extended Data Fig. 6i, j). Similarly, acetate and propionate, two other Olfr78 ligands that can also stimulate carotid sinus nerve activity[14,26], had little effect in $Olfr78^{-/-}$ mutants (Extended Data Fig. 6i, j). We conclude that carotid body activation by lactate and two other Olfr78 ligands is mediated by Olfr78.

Our results support a model in which decreased blood oxygen is sensed by the carotid body through an increase in production and secretion of lactate, which binds to Olfr78 on glomus cells and induces calcium transients that increase signaling to afferent nerves to stimulate breathing (Fig. 4f). In the model, changes in blood oxygen are not detected directly by glomus cells, but indirectly through a metabolite (lactate) whose production is regulated by oxygen availability. This explains why drugs and mutations that inhibit the mitochondrial electron transport chain, preventing oxygen utilization and causing lactate buildup, mimic the effect of hypoxia on carotid body activity and breathing, and supports the mitochondrial hypothesis of carotid body oxygen sensing (Extended Data Fig. 1d, e). Thus, the Olfr78 pathway measures a metabolic state that integrates oxygen availability and demand and serves as a sentinel that signals, and attempts to stave off, an impending oxygen crisis, whereas the HIF-1 pathway senses oxygen directly (through prolyl hydroxylases that use oxygen to modify HIF-1 stability) and operates later and more broadly to deal with the crisis[1].

What is the source of the lactate that activates Olfr78? Lactate is produced by all cells in the body when oxygen declines: the blockage of mitochondrial electron transport leads to accumulation of upstream metabolites such as pyruvate, which is rapidly converted to lactate and then effluxed from cells (Extended Data Fig. 1e). Upon hypoxia exposure, lactate can almost double in blood within minutes (Fig. 4b and Extended Data Fig. 7h), and it accumulates in blood when inspired oxygen drops to levels that can activate carotid body signaling and hyperventilation[27]. Besides blood, another potential source of lactate is the carotid body itself, as tissue lactate levels also increase rapidly in hypoxia, doubling within 30 seconds in some tissues[5,6]. Mitochondria of carotid body cells are highly sensitive to hypoxia compared to other tissues (Extended Data Fig. 1d), so when blood oxygen levels decline, carotid body cells should be among the first to produce lactate, ideal for Olfr78 sentinel function. Because lactate is transported out of cells with H^+, glomus cells would be exposed to increases in both extracellular lactate and H^+, which could activate acid-sensitive channels (ASICs, TASKs) synergistically with Olfr78 to stimulate glomus cells[2,28,29]. Lactate/Olfr78 signaling may act with H^+ and perhaps other signals and pathways to promote the full carotid body response to hypoxia, explaining the small residual response to hypoxia detected in $Olfr78^{-/-}$ mutants (Fig. 3h and Extended Data Fig. 6a–h).

In addition to the carotid body, Olfr78 is expressed in a number of other oxygen-responsive tissues such as heart and lung[9,13,14], and it is required for maintaining normal blood pressure[14]. We speculate that lactate and Olfr78 serve as a general signal and sensor of hypoxic and altered metabolic states to control physiological responses. Nevertheless, some acute responses to hypoxia, such as reduced locomotion, regular breathing, and metabolic depression, are independent of *Olfr78*. It may be valuable to develop synthetic agonists and antagonists for Olfr78 for therapeutic control of breathing[30] and other responses it controls.

Genomic studies detect ectopic expression of other ORs in addition to *Olfr78* and *Olfr558*, and some of these appear to be functional[9,10,14]. Downstream signaling in the carotid body may differ from that in olfaction (Extended Data Table 2), and it will be important to elucidate the full Olfr78 signal transduction cascade in the carotid body and its integration with other pathways activated by hypoxia and other sensory stimuli. Although olfactory receptors were first identified for their role in smell, they may be involved in myriad chemosensory pathways detecting endogenous and exogenous ligands throughout the body.

Methods

Animals

All experiments with animals were approved by the Institutional Animal Care and Use Committee (IACUC) at the Stanford University School of Medicine.

C57/BL6, Stock #027 (Charles River) was used as wild type for microarrays and RNA sequencing. Other mouse strains used were:

Olfr78 knock-in reporter: MOL2.3-*IGITL*, kindly shared by Ron Yu (Stowers Institute)[11]

Olfr78 knock-in mutant/reporter: B6; 129P2-*Olfr78^{tm1Mom}*/MomJ, Stock #006722 (JAX)[16]

Olfr558 mutant/reporter: B6129S5-*Olfr558^{tm1Lex}*, Stock #TF0586 (Taconic)

Th-Cre driver: B6.FVB(Cg)-*Tg(Th-cre)^{FI172Gsat}*/Mmucd, Stock #031029-UCD (MMRRC)[31]

Th-Cre driver: *Th^{tm1(cre)Te}*, kindly shared by Karl Deisseroth (Stanford)[32]

ROSA-GCaMP3: B6;129S-*Gt(ROSA)26Sor^{tm38(CAG-GCaMP3)Hze}*/J, Stock #014538 (JAX)[33]

ROSA-tdTomato: B6;129S6-*Gt(ROSA)26Sor^{tm9(CAG-tdTomato)Hze}*/J, Stock #007905 (JAX)[34]

Adult animals were used in all experiments, unless indicated otherwise. To control for sex differences, only female animals were used in physiology and behavioral experiments. Randomization and blinding were not used, in part because the *Olfr78* mutant allele is genetically linked to a coat color variant. All data include animals from multiple litters.

Carotid body and adrenal medulla RNA purification

Adult C57/BL6 animals were anesthetized with isoflurane and decapitated, and carotid bifurcations and adrenal glands were dissected immediately and transferred to RNA*later* solution (Life Technologies) on ice. Carotid bodies and adrenal medullas were finely dissected from these tissues. From each animal, 1–2 carotid bodies and 1 adrenal medulla were obtained and stored in RNA*later* at 4°C for up to 2 days. For each RNA purification, 18 carotid bodies and 10 adrenal medullas from 10 animals were pooled and processed using the RNeasy Micro Kit (Qiagen). Tissue pieces were disrupted in a guanidine-isothiocyanate lysis buffer (Buffer RLT, Qiagen) using a glass tissue grinder (Corning), homogenized using a 20G needle and syringe, and purified by silica-membrane columns. RNA quality was assessed by electrophoresis on a Bioanalyzer using the RNA 6000 Pico Kit (Agilent). The average RNA Integrity Numbers (RIN) for carotid body and adrenal medulla samples were 7.2 and 9.0, respectively.

Microarrays

Total RNA (>30 ng/sample) was processed using the 3' IVT Express Kit (Affymetrix) to make biotinylated amplified RNA (aRNA) by cDNA synthesis and *in vitro* transcription. aRNA was fragmented and hybridized to the GeneChip Mouse Genome 430 2.0 Array (Affymetrix) containing 45,000 probe sets targeting >34,000 mouse genes. aRNA synthesis, hybridization, and scanning were performed by the Stanford PAN Facility. Analysis of microarray data was performed using Expression Console and Transcriptome Analysis Console software (Affymetrix).

RNA sequencing

Using the Amino Allyl MessageAmp II aRNA Amplification Kit (Ambion), unlabeled aRNA was generated from total RNA (30–50 ng/sample) by an engineered M-MLV reverse transcriptase to make cDNA followed by *in vitro* transcription. aRNA was fragmented by RNA Fragmentation Reagents (Ambion), a buffered zinc solution, for 1.5 minutes at 70°C. First and second strand cDNA synthesis, end repair, 3'-dA tail addition, and adaptor ligation were performed using the standard protocol from Illumina with adaptor oligonucleotides from Illumina, First Strand Buffer, SuperScript III reverse transcriptase, and Second Strand Buffer from Invitrogen, and RNaseH, DNA polymerase I, T4 DNA polymerase, Klenow DNA polymerase, T4 polynucleotide kinase, Klenow fragment (3'-5' exo-), and T4 DNA ligase from New England Biolabs. Modified cDNA libraries were resolved by electrophoresis in 2% low-melting agarose (Lonza) gels. For each sample, a region of the lane corresponding to ~200 base pairs was excised and purified by the QIAquick Gel Extraction Kit (Qiagen) using silica-membrane columns. Modified cDNA libraries were further amplified by PCR for 20 cycles using Phusion DNA polymerase (New England Biolabs). cDNA concentration and size were determined by electrophoresis using the High Sensitivity DNA Kit on the Bioanalyzer (Agilent), and samples were diluted to 4 pM for sequencing.

DNA clusters were generated using the Cluster Generation Kit according to manufacturer instructions (Illumina). Samples were then sequenced on the Illumina Genome Analyzer II

using the 36-Cycle SBS Reagent Kit v2 (Illumina) run for 38 cycles. Each cDNA library was run in one lane, and data presented in this study are from two separate runs.

Sequences were aligned to the RefSeq database using Bowtie 0.9.8, allowing up to 4 mismatches in the first 32 bases for a sequence to be assigned to a specific gene ID. Reads that mapped to multiple isoforms of a gene were randomly assigned to one isoform, and counts for multiple mRNA isoforms for the same gene were combined for analysis. The number of aligned reads per 10^7 aligned reads was calculated after adding 1 read to every gene and sample in order to avoid dividing by 0 when calculating ratios between AM and CB frequencies (Fig. 1a and Extended Data Fig. 2a). Reads per kilobase per million (RPKM) values were calculated by using the length of the mRNA, or the longest mRNA isoform for genes that have multiple isoforms, in RefSeq (Fig. 1b and Extended Data Fig. 2b).

X-gal staining

Whole mount carotid bifurcations and adrenal glands were harvested, cleaned, and fixed in 4% paraformaldehyde (PFA)/PBS (pH 7.4) for 10 minutes at room temperature. After washing with PBS, tissue was transferred to a solution of X-gal (1 mg/ml), potassium ferricyanide (5 mM), potassium ferrocyanide (5 mM), magnesium chloride (2 mM), and NP-40 (0.02%) in PBS and incubated overnight at 37°C. Samples were visualized on a Leica MZ12 stereomicroscope. Representative data reflect tissue samples from ten *Olfr78-GFP-taulacZ*$^{Tg/Tg}$ (Fig. 1c–f, i-k) and three *Olfr558*$^{lacZ/lacZ}$ (Extended Data Fig. 3e) animals.

For carotid bifurcation samples shown in section (*n*=3 animals), tissue was fixed in 4% PFA/PBS for 10 minutes at room temperature and equilibrated in 30% sucrose overnight at 4°C. Tissue was then embedded in optimum cutting temperature compound (O.C.T., TissueTek) and stored at −80°C. Sections were cut at 10 μm using a Leica CM3050S cryostat. X-gal solution was added onto sections on slides and incubated overnight at 37°C. Slides were mounted in Mowiol 4–88 (Polysciences) with 1,4-diazabicyclo[2.2.2]octane (DABCO, 25 mg/ml, Sigma-Aldrich) or Permount (45% polymer of α-pinene, β-pinene, dipentene, β-phellandrene/55% toluene, Fisher) and visualized on a Zeiss Axiophot fluorescence microscope.

For adult brain tissue, two animals were perfused through the heart with PBS followed by 4% PFA/PBS using a syringe. Whole brains were dissected from the head, and fixed again for 30 minutes in 4% PFA/PBS at 4°C. After equilibration in 30% sucrose overnight at 4°C, samples were embedded in O.C.T. (TissueTek) and sectioned at 80 μm using a Leica CM3050S cryostat. Slides were then incubated with X-gal overnight at room temperature and visualized on a Leica MZ12 stereomicroscope.

Immunostaining

Tissue was fixed in 4% PFA/PBS at room temperature for 10 minutes and equilibrated in 30% sucrose overnight at 4°C. Tissue was embedded in O.C.T. (TissueTek) and stored at −80°C. Sections were cut at 10 μm using a Leica CM3050S cryostat and incubated with primary antibodies overnight at 4°C. Primary antibodies were rabbit anti-TH (Abcam,

ab112), chicken anti-GFP (Abcam, ab13970), rat anti-CD31 (BD Pharmingen, 553370), chicken anti-β-galactosidase (Abcam, ab9361), and mouse anti-smooth muscle actin (Sigma, A5228) used at 1:500. Mouse anti-smooth muscle actin antibody was directly conjugated to Cy5 NHS ester (GE Healthcare), and unbound dye was removed on a P-30 gel exclusion column (BioRad)[35]. Incubation with secondary antibodies was 45 minutes at room temperature. Secondary antibodies were conjugated to either Alexa Fluor 488, Alexa Fluor 555 (Life Technologies), or DyLight 488 (Jackson ImmunoResearch). Staining with 4',6-diamidino-2-phenylindole (DAPI; 1 ng/ml, Life Technologies) was performed after incubation with secondary antibodies for 5 minutes at room temperature. Sections were mounted in Mowiol 4–88 (Polysciences) with DABCO (25 mg/ml, Sigma-Aldrich) and visualized on a Zeiss Axiophot fluorescence microscope. Tissue samples from three or more animals were stained for representative data shown (Fig. 1g, h, Fig. 3a, b, and Extended Data Fig. 3a–c, f–h).

Electron microscopy

Carotid bifurcations were harvested from adult animals and transferred to fixation solution (4% PFA and 2% glutaraldehyde in PBS) for 1 hour at room temperature. During fixation, excess tissue was trimmed away to retain the carotid body and carotid arteries. Samples were post-fixed with osmium tetroxide for 1.75 hours at 4°C, washed three times with cold double distilled H_2O, and incubated with 1% uranyl acetate overnight at 4°C. On the next day, samples were serially dehydrated in ethanol (50%, 70%, 100%, 100%) for 10 minutes per step and washed with propylene oxide for 15 minutes, all at room temperature. Samples were then transferred to 1:1 propylene oxide: Epon (Electron Microscopy Services) for 1 hour, 1:2 propylene oxide: Epon for 45 minutes, and 100% Epon, all at room temperature. Once samples were embedded in 100% Epon, blocks were baked overnight at 65°C.

To locate the carotid body in the embedded tissue, sections were cut at 2 μm using glass knives on a Leica Ultracut S microtome and stained with Toluidine Blue (Sigma-Aldrich) for visualization of tissue histology. Once the carotid body was reached, 17 nm sections were cut using a diamond blade for transmission electron microscopy. Sections were visualized on a JEOL TEM1230 transmission electron microscope equipped with a Gatan 967 slow-scan, cooled CCD camera. Two sections at different levels in the carotid body were examined for each sample. All sectioning and imaging procedures were performed at the Stanford Cell Sciences Imaging Facility-Electron Microscopy Core.

Whole body plethysmography

Unrestrained, unanesthetized adult animals were transferred to a whole body plethysmograph (450 ml, Model PY4211, Buxco) connected to a MAXII preamplifier unit and computer running BioSystem XA software (Buxco). To reach stable baseline ventilation, animals were acclimatized to the chamber for more than 30 minutes in control gas conditions before exposure to hypoxia or hypercapnia. Three pulses of hypoxia or hypercapnia lasting 5 minutes each were performed with 10-minute recovery periods in control conditions. Gas mixtures for control, hypoxia, and hypercapnia were 21% O_2/79% N_2, 10% O_2/90% N_2, and 5% CO_2/21% O_2/74% N_2, respectively (Praxair). Flow rates were

1.5 L/min during measurement periods and 11–12 L/min during 1-minute ramp periods between gas mixtures.

Ventilatory parameters were collected and calculated by BioSystem XA software (Buxco). Tidal volumes were calculated according to Drorbaugh and Fenn[36] with manual input of environmental conditions, such as room and chamber temperature, humidity, and barometric pressure. To enrich for measurements of regular breaths, criteria were set in the software to accept a breath if (1) inspiratory time was greater than 0.07 seconds, (2) expiratory time was less than 10 seconds, (3) calculated tidal volume was greater than 0.05 ml, and (4) volume balance between inspiration and expiration was less than 50%. Under these conditions, virtually all breaths were accepted during very regular breathing in hypoxia and hypercapnia. Fifteen breaths were averaged for each line of data, and lines of data for each period of control or stimulus were averaged, excluding lines that had more than two observed events of sniffing, grooming, or movement among the accepted breaths. Ventilatory parameters over all periods of control or stimulus were averaged for each animal and presented in the figures. Most animals were tested two times within one week with good reproducibility, and measurements were averaged. Numbers of animals tested were comparable to other published work[37–40]. While there was no formal randomization, different numbers, genotypes, and litters were tested in different orders on multiple days over several months. For the animals used in our study, body weight did not correlate with respiratory rate, tidal volume, or minute ventilation in wild-type animals, mutant animals, or all animals together (correlation coefficients 0.001 R^2 0.289, 0.996 P 0.293).

Blood gas and lactate measurements

For blood testing under anesthetized conditions, animals were transferred to individual cages the morning of testing and allowed to acclimate for at least 4 hours. This was designed to avoid repeated cage handling and removal of other animals from the same cage, procedures that have been shown to increase stress hormones and blood lactate levels in rodents[41]. Animals were quickly anesthetized with 3% isoflurane in 100% O_2 in an acrylic container and maintained in 1.5–2% isoflurane in 21% O_2/79% N_2 or 10% O_2/90% N_2 (Praxair) at 2 L/min through a nose cone. Body temperature was maintained at 37°C using a heating pad with feedback temperature controller (Physitemp Instruments). The right carotid artery was surgically isolated and cut, and 200–250 µl of blood was collected using a heparinized syringe. An aliquot (~100 µl) of arterial blood was immediately transferred to a CG4+ cartridge for measurement of blood gases and lactate using an i-Stat Portable Clinical Analyzer (Abbott). Time from beginning of surgery to blood collection was ~3 min, during which the hypoxic ventilatory response was still robust under our conditions (data not shown). For some animals, arterial blood was also transferred to a test strip for lactate analysis using a Lactate Scout analyzer (EKF Diagnostics). We found good correlation between lactate measurements of the same blood sample from anesthesized animals using i-Stat and Lactate Scout analyzers (n=11, R^2=0.92, P<0.0001).

For blood lactate measurements in unanesthetized conditions, animals were transferred to individual cages at least one day before the first day of testing. Animals in their housing cage were moved into a hypoxia control glove box set to 21% O_2 or 10% O_2 balanced by N_2

(Coy Laboratory Products). After 1 min in the airlock, the cage was moved into the glove box, and the lid was opened for another 3 min. Then the animal was transferred to a tail vein restrainer (Braintree Scientific), and the tail artery was punctured with a 27G½ needle. Blood was then directly transferred to a test strip for measurement of lactate using a Lactate Scout analyzer. The total time of animals in the glove box before blood testing was 4–5 min. Due to handling stress increasing blood lactate concentrations[41] and causing more variable blood lactate measurements in awake conditions, animals were kept in the same room and tested on 4 separate days for 2 days each of 21% O_2 or 10% O_2 exposure. Results for each animal and oxygen condition were then averaged. One *Olfr78*^{+/+} animal was excluded because of excessive handling stress due to long blood collection on 2 days.

Body temperature measurements

Unanesthetized animals were transferred to a tail vein restrainer (Braintree Scientific), and body temperature was measured using a rectal temperature probe and animal temperature controller (Physitemp Instruments) in room air (21% O_2) or in 10% O_2 in a hypoxia control glove box (Coy Laboratory Products). Data were collected in 21% O_2 at 1 hour before transfer to the hypoxia control glove box and at 2 and 5 minutes in 10% O_2 inside the glove box. An airlock was used to transfer the animal into the glove box for a ramp time of 1 minute from 21% O_2 to 10% O_2.

Metabolic measurements

Unrestrained, unanesthetized animals were transferred to the same chamber used for plethysmography that was sealed to only allow airflow in from the side port and out from a bottom port on the opposite side. Metabolic measurements were collected using an Oxymax open circuit indirect calorimeter (Columbus Instruments) with an electrochemical oxygen sensor modified to measure two ranges around 21% O_2 and 10% O_2. Flow was set to 0.6 L/min from gas mixtures of 21% O_2/79% N_2 and 10% O_2/90% N_2 (Praxair). Measurements were taken every 30 seconds. For 21% O_2, animals were allowed to acclimate to the chamber for 10 minutes, and data is shown for 10–15 minutes after the start of measurements. For 10% O_2, animals became calm more quickly, and data is shown for 5–10 minutes after the start of measurements, a duration we found necessary for the system to stabilize to 10% O_2 after opening the chamber.

Measurements of oxygen in perfusion

Measurements of oxygen concentrations of the perfusion solution in the recording chamber were performed using a Clark style oxygen electrode (Unisense). Because voltage readings for the sensor were observed to be highly temperature-dependent, the sensor was calibrated at the temperature of the relevant protocol, which was 33–34°C for electrophysiology and room temperature for calcium imaging.

Carotid sinus nerve recordings

Animals were terminally anesthetized with isoflurane, perfused through the heart with ice-cold artificial cerebrospinal fluid (ACSF, pH 7.4) composed of 119 mM NaCl, 5 mM KCl, 2.5 mM $CaCl_2$, 1.3 mM $MgSO_4$, 1 mM NaH_2PO_4, 26.2 mM $NaHCO_3$, and 11 mM glucose

previously bubbled with 95% O_2/5% CO_2 (Praxair), and decapitated. Both carotid bifurcations were then dissected in ice-cold ACSF and transferred to a recording chamber (3 ml), where they were superperfused with ACSF continuously bubbled with 95% O_2/5% CO_2 (Praxair) at a flow rate of 13.3 ml/min by gravity and maintained at 33–34°C. The carotid sinus nerve was carefully exposed and cut near the point where it branches from the glossopharyngeal nerve. The cut end was pulled into a tightly fitting glass suction micropipette[38,40], and voltage was recorded relative to a reference in the bath using an Axoclamp 2A electrometer (Molecular Devices) in Bridge mode. The voltage signal was amplified 1000X (10X on the Axoclamp and 100X on a Brownlee Precision Model 440 instrumentation amplifier), filtered (0.2–3 kHz), and digitized at 10 kHz on a National Instruments MIO15E-2 analog-to-digital converter. Data were stored and displayed using in house software written in LabView (National Instruments).

If spikes were not observed at baseline for the first carotid sinus nerve, the second carotid bifurcation was dissected and recorded. One-second sweeps were acquired continuously through the entire time course, and only one carotid sinus nerve recording per animal was included in the data presented. Hypoxia stimulus was delivered by changing the gas bubbling the ACSF to 95% N_2/5% CO_2 (Praxair) for 8 min. Under these conditions, PO_2 levels in the recording chamber started at 625 mmHg and decreased to a low of 60 mmHg by 9 min after the start of bubbling with 95% N_2/5% CO_2 (Fig. 3h). Solutions of lactate, acetate, and propionate (30 mM, pH 7.4) were made by equimolar substitution of NaCl in ACSF with sodium salts of L-lactate, acetate, and propionate, respectively. Low pH solution (pH 7.0) was made by lowering the $NaHCO_3$ in ACSF from 26.2 mM to 11.9 mM with an equimolar increase in NaCl[38]. These solutions were continuously bubbled with 95% O_2/5% CO_2 (Praxair) at the reservoir, maintaining the oxygen concentration of the solution in the chamber at PO_2=625 mmHg. All preparations were stimulated with bolus injections of 25–50 μl sodium cyanide (20 mM) at the end of the experiment to confirm that the nerve was active.

Recordings were analyzed offline using Spike2 software (Cambridge Electronic Design). To measure action potential frequency, we analyzed a one-second period of data every minute. A single threshold was used for spike determination and set empirically for each time course by moving the threshold through a range of values until the spike count stabilized through several intervals of 0.001 mV and then dropped off for data at time=0 and 9 min (hypoxia) or all time points scored (acetate, propionate, lactate, and low pH). The lowest threshold value in the stable range was applied to all sweeps of a stimulus analyzed for each recording. Because we noticed that spikes close together or with low amplitudes were often missed by the software, we also manually counted spikes for the same sweeps analyzed by software. Two recordings were excluded due to low signal to noise precluding accurate analysis. In two experiments, we also applied 7.5 μM tetrodotoxin (TTX) to block voltage-gated sodium ion channels during hypoxia exposure as an additional confirmation that events being scored were action potentials (Extended Data ig. 6c, d).

pCI-Rho-Olfr78 plasmid construction and expression

The pCI-Rho-Olfr78 plasmid was made by PCR amplifying the Olfr78 coding region from a pCMV6-Olfr78 plasmid (OriGene) using forward primer 5'-ATTGCCGAATTCATGAGTTCCTGCAACTTCACC-3' and reverse primer 5'-ATTGCCGCGGCCGCTCACGTGTTTCCCCCAGCTTCAA-3', adding EcoRI and NotI restriction sites. The Olfr78 PCR fragment was then digested with EcoRI and NotI and cloned into a pCI-Rho backbone cut from a pCI-Rho-Olfr62 plasmid (gift of Hiroaki Matsunami, Duke University). Cell-surface expression of Rho-epitope-tagged Olfr78 protein in HEK293T cells was confirmed by immunostaining as described[42]. Cytoplasmic GFP (co-transfection marker) was expressed from a TBC1D25::eGFP plasmid (gift of Suzanne Pfeffer, Stanford University).

Luciferase assay

HEK293T cells were grown and seeded into 96 well plates as described[42]. On the next day, cells were transfected with RTP1S, $G_{\alpha15\text{-olf}}$ (gifts of Hiroaki Matsunami, Duke University), pCMV6-Ric8b (Origene), pCRE-Luc (Agilent), and pSV40-RL (Promega) plasmids and either pCI-Rho-Olfr78 or pCI (Promega). The Rho tag on Olfr78 and RTP1S were used to enhance localization of Olfr78 to the plasma membrane. $G_{\alpha15\text{-olf}}$ and Ric8b were included as downstream effectors that couple to ORs to increase cAMP production upon OR activation. Two transcriptional luciferase reporters, one constitutive (*Renilla*, pSV40-RL) and one inducible by cAMP (firefly, pCRE-Luc) were transfected to report increased cAMP levels upon OR activation[42].

Five hours after transfection, media was decanted and replaced with 50 μL/well MEM without phenol red (Life Technologies). After thirty minutes, 25 μL of chemicals were added to each well to achieve the indicated final concentrations, and cells were incubated for 2 hours. Sodium salts of chloride, L-lactate, propionate, and acetate (Sigma) were used. The duration of transfection and stimulation was shortened because we observed that transfection of cells with pCI-Rho-Olfr78 overnight caused a large increase in firefly luciferase activity in the absence of added chemicals (data not shown), suggesting that lactate or some other molecule released from cells and/or a component of the transfection mixture could stimulate Olfr78 activity.

Reagents to detect firefly and *Renilla* luciferase activity (Dual-Glo Luciferase Assay System, Promega) were added at 20 μl/well[42]. Luminescence was measured using an Infinite M1000 (Tecan) microplate reader and data acquired by Magellan Data Analysis Software (Tecan). Two readings were collected for each plate and luciferase reagent, and firefly to Renilla ratios were averaged. Data was from experiments conducted over three days. For dose response curves in Fig. 4a and Extended Data Fig. 7d–f, ratios were normalized to the highest and lowest average values for a given condition across all plates on each day.

The HEK293T cell line (gift of Suzanne Pfeffer, Stanford University) was not authenticated or tested for mycoplasma contamination.

Calcium imaging

Th-Cre; ROSA-GCaMP3 animals expressing GCaMP3 in glomus cells were generated using two *Th-Cre* drivers[31–33]. Both *Th-Cre* lines drove expression in glomus cells, as confirmed by *Th-Cre; ROSA-tdTomato* animals[34], but the BAC-transgenic *Th-Cre* driver (MMRRC) required two copies of *ROSA-GCaMP3* reporter for robust expression[31]. For whole mount preparations, carotid bifurcations were dissected from transgenic animals and transferred to 0.5% glucose/PBS bubbling 100% O_2 on ice. Surrounding tissue was removed to expose the carotid body attached to the carotid artery. The carotid body was incubated in a physiological buffer (115 mM NaCl, 5 mM KCl, 24 mM $NaHCO_3$, 1 mM $MgCl_2$, 2 mM $CaCl_2$, 11 mM glucose[43]) at 37°C in a tissue culture incubator with 5% CO_2 before transfer to the recording chamber for imaging.

For tissue slices, carotid bifurcations were dissected and transferred to a modified Tyrode's solution (148 mM NaCl, 2 mM KCl, 3 mM $MgCl_2$, 10 mM HEPES, 10 mM glucose), pH 7.4 on ice[44]. Carotid bodies were then isolated and embedded in 3% low melt agarose (Lonza) in a sample holder (Precisionary Instruments). Tissue slices were cut at 100 μm using a Compresstome VF-200 (Precisionary Instruments). Samples were then transferred to culture medium composed of DMEM with 10% FBS, 1% penicillin/streptomycin, and insulin-transferrin-selenium (Life Technologies) and incubated in a tissue culture incubator at 37°C with 5% CO_2 for at least 24 hours before calcium imaging according to established protocols[44].

At baseline, the carotid body was superperfused with physiological buffer bubbling 95% O_2/5% CO_2 at 3.75 ml/min using a Reglo analog tubing pump (Ismatec), maintaining the oxygen concentration of the solution in the chamber at PO_2=600 mmHg. Hypoxia was generated by bubbling physiological buffer with 95% N_2/5% CO_2. Lactate solution (30 mM) was made by equimolar substitution of NaCl with sodium L-lactate. Lactate and cyanide solutions were bubbled with 95% O_2/5% CO_2. To switch between stimuli, the flow rate was increased to 7.5 ml/min for 2 minutes.

The carotid body was imaged on a Prairie Ultima XY two-photon rig built around an Olympus BX-61W upright microscope at the Stanford Neuroscience Microscopy Service. Using a water immersion 60X objective, Z-stacks at 2 μm steps were collected at 1024 × 1024 pixels resolution for 70–100 μm of tissue. Two stacks were collected for hypoxia and lactate stimuli and intervening buffer recovery periods for whole mount samples. Images were analyzed using ImageJ. Regions of interest corresponding to individual glomus cells were defined by the images with the strongest fluorescence. Average fluorescence intensities were calculated for each region of interest, and values were averaged for stimulus and buffer periods with more than one stack. Cells that had very high levels of fluorescence at the start of the experiment were excluded from our analysis of data from whole mount samples[43] because these cells showed dramatic declines in baseline fluorescence after hypoxia and lactate stimulation (data not shown). Data presented are from 2 samples from 2 different animals performed on separate days.

Data analysis and statistics

Data analysis and statistical tests were performed using Microsoft Excel and GraphPad software. GraphPad Prism 6 was used to fit dose-response curves using a variable slope model and to calculate EC_{50} values. All data are biological replicates, and quantitative data with error bars are presented as mean ± standard error of the mean (s.e.m.) with the exception of Extended Data Fig. 7c, which is presented as percent ± standard error of percentage. Groups compared by parametric tests fit the assumption for normal distribution as determined by the Shapiro-Wilk test with the critical W value set at 5% significance level. All t tests shown are two-sided, and variances of sample groups compared were similar. No statistical method was used to predetermine sample size.

Extended Data

a

b

c

d

e
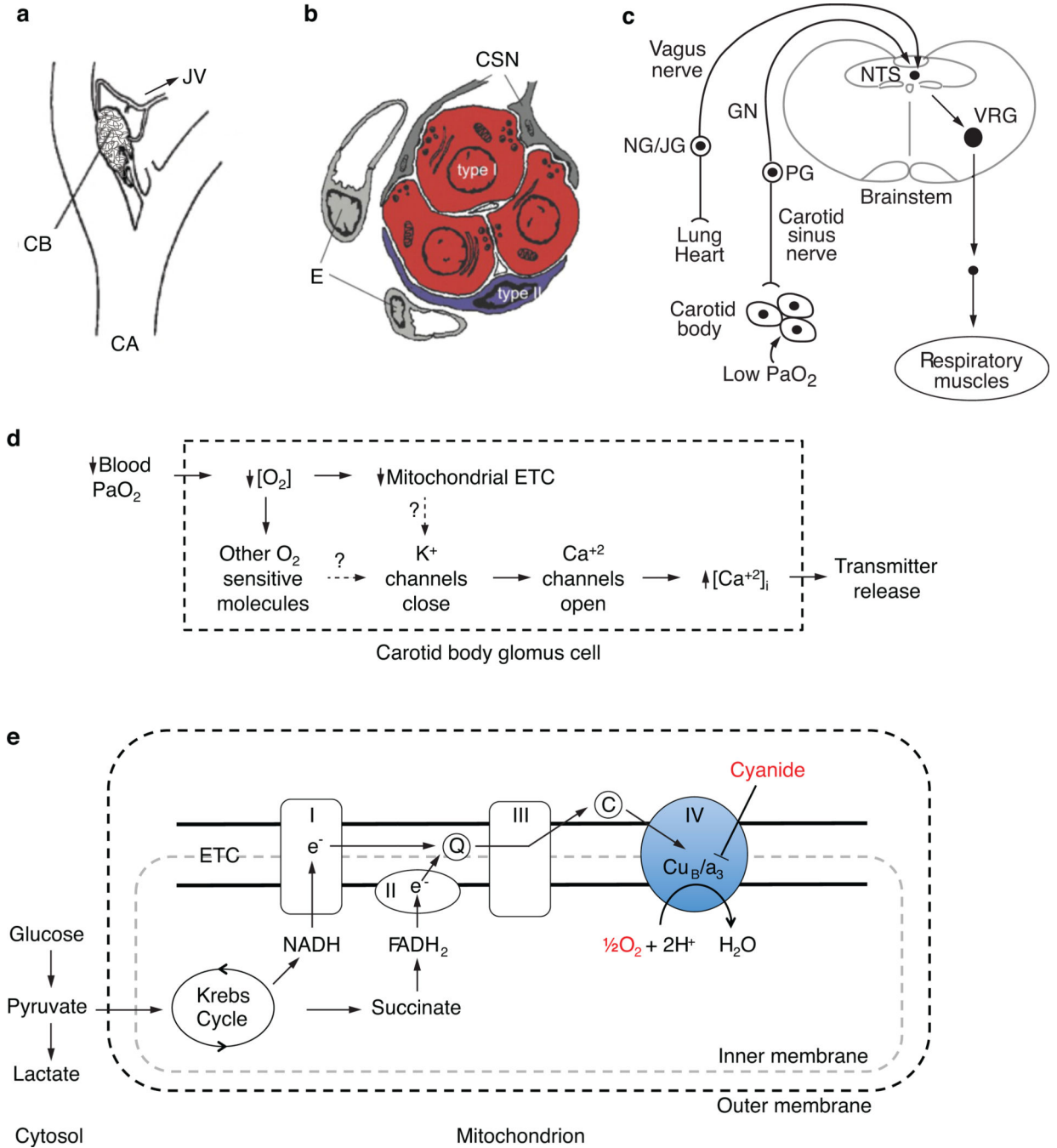
Extended Data Figure 1. Model of oxygen sensing by the carotid body and the mitochondrion
a, Anatomy and blood supply of the carotid body (CB). CB is located bilaterally at bifurcation of carotid artery (CA) in the neck. Its location can be variable as well as the source of its blood supply, which can come from branches of nearby internal and external carotid, occipital, pharyngeal arteries. Blood flows through fenestrated capillaries close to clusters of Type I glomus cells and drains from CB into jugular vein (JV) on ventral side[2].

Panel adapted from ref[45]. **b**, Cellular organization of CB. CB is composed of several cell types, including Type I glomus cells (red) that sense changes in blood oxygen and are organized in clusters, Type II sustentacular cells (blue) that resemble neuroglia and surround glomus cell clusters, carotid sinus nerve (CSN) fibers that innervate glomus cells, and endothelial (E) and smooth muscle cells (not shown) that form the tortuous vasculature[2]. Panel adapted from ref[45]. **c**, Oxygen-sensing respiratory circuit. The primary chemoreceptor for blood oxygen is the carotid body. A decrease in PaO_2 of arterial blood from normoxia (100 mmHg) to hypoxia (<80 mmHg) stimulates glomus cells to signal the carotid sinus nerve, a branch of glossopharyngeal nerve (GN) with cell bodies in petrosal ganglion (PG). Axons of the GN terminate in nucleus tractus solitarius (NTS) in brainstem, a site of many converging afferent inputs[2]. The signal from NTS is transmitted to ventral respiratory group (VRG) that includes preBötzinger complex, a region essential for respiratory rhythm generation. From VRG, neurons project to premotor and motor neurons that innervate respiratory muscles, such as diaphragm and intercostal muscles[46]. In addition to carotid body, vagus nerve afferents can also contribute to respiratory behaviors under specialized conditions[39]. The vagus nerve innervates heart and lung and oxygen-sensitive cells of aortic body[70]. Panel adapted from ref[46]. **d**, A current model of acute oxygen sensing by carotid body. A decrease in PaO_2 in blood causes a decrease in O_2 concentration inside carotid body glomus cells. This causes a decrease in activity of mitochondrial electron transport chain (ETC)[47] and changes in other putative oxygen-sensing pathways, such as oxygen-sensitive K^+ channels[48,49], heme oxygenase[50], AMP kinase[51], and hydrogen sulfide signaling[37]. These changes are hypothesized to converge on oxygen-sensitive K^+ channels, which close in hypoxia and depolarize the plasma membrane. Depolarization then opens voltage-gated Ca^{+2} channels, leading to an increase in intracellular calcium that stimulates transmitter release to carotid sinus nerve to increase breathing[2]. Mitochondria of carotid body cells are highly sensitive to hypoxia compared to other tissues, as assayed by imaging of mitochondrial membrane potential, NADH levels, and spectral properties[23,52–54]. Drugs and mutations that inhibit the ETC mimic the effect of hypoxia on carotid body activity and breathing[23,55–59]. **e**, Regulation of lactate production by oxygen. In normoxia, pyruvate produced by glycolysis is transported into mitochondria and efficiently used in Krebs cycle to supply electrons to ETC to produce ATP. In hypoxia, lack of oxygen to act as the final electron acceptor limits electron transport, causing pyruvate to build up and become converted to lactate[5,6,27]. The ETC poison cyanide inhibits the heme a3 subunit of cytochrome c oxidase to prevent transfer of electrons to oxygen, leading to lactate accumulation even in presence of adequate oxygen[60]. Cytosolic lactate accumulation results in transport of lactic acid (lactate and H^+) out of the cell by monocarboxylate transporters[6,61]. In normoxia, lactate concentrations in blood, tissue, and tissue interstitium are 1–5 mM[62,63].
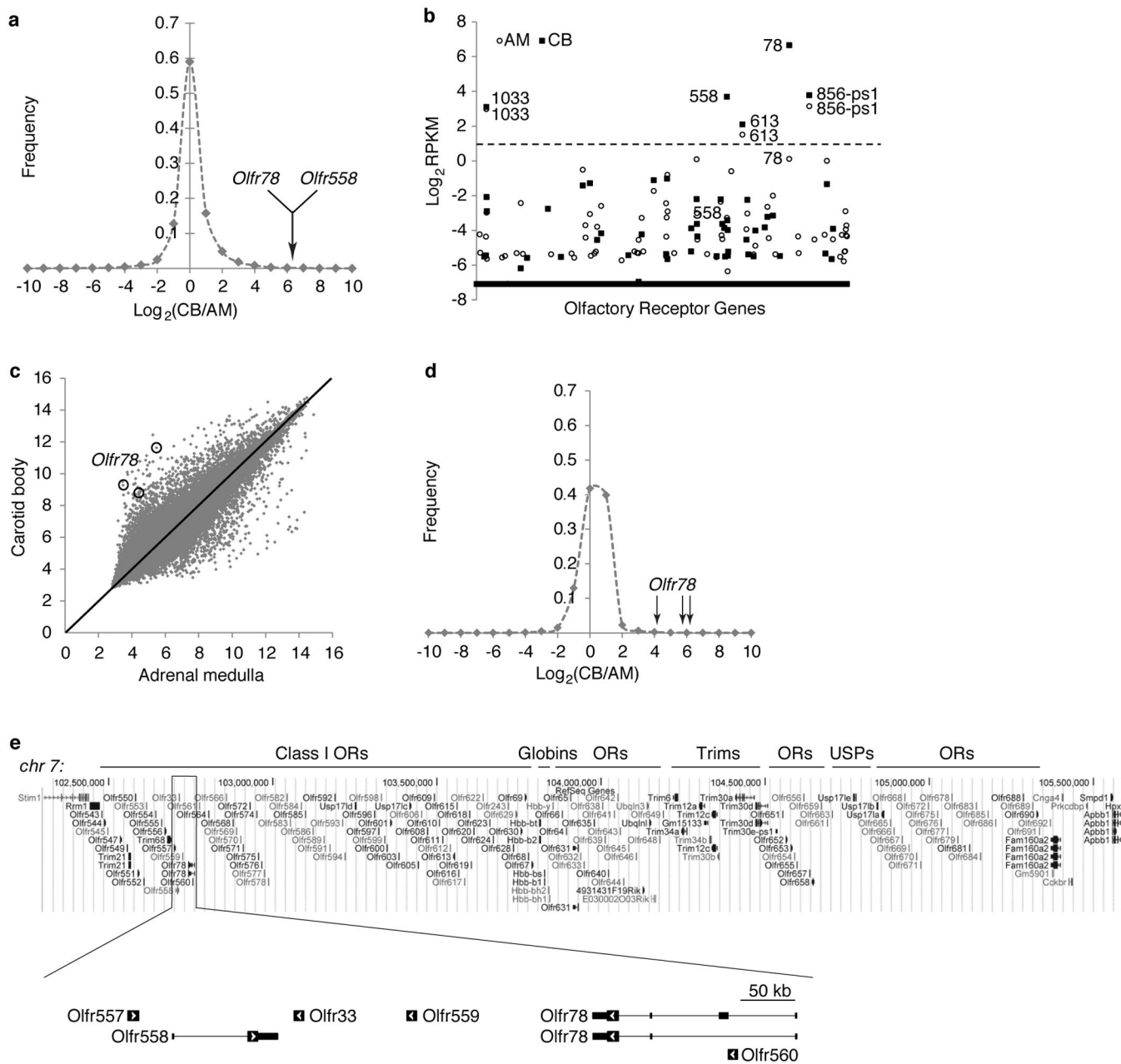
Extended Data Figure 2. RNA sequencing and whole genome microarrays detect *Olfr78* transcripts enriched in the carotid body

a, Histogram of frequency of genes for different levels of expression enrichment in carotid body (CB) relative to adrenal medulla (AM) by RNA sequencing. $Log_2(CB/AM)$ values are shown, with data binned for every log_2 interval of 1.0 centered at integers. **b**, Plot of log_2 values of reads per kilobase per million (RPKM) in CB and AM of all 1,126 olfactory receptor (OR) genes annotated in RefSeq shown in alphanumerical order. The five OR genes expressed at RPKM > 2 (dashed line) are indicated. Samples that had no transcripts are plotted at a value of −7.1, just below the smallest RPKM value for ORs. Data presented in Supplementary Table 1. **c**, Comparison of expression levels of >34,000 genes in adult mouse

CB and AM by whole genome microarrays. Plot shows $\log_2$ of the ratio for CB relative to AM of the fluorescence intensity values for the 45,000 probe sets. The three probe sets for *Olfr78* transcripts are indicated (circles). Expression of *Olfr78* was significantly different between CB and AM for all three probe sets (*P*<0.05 by ANOVA with false discovery rate control). **d**, Histogram of the frequency of genes for different levels of expression enrichment in CB relative to AM in microarray data. $\log_2$(CB/AM) values are shown, with data binned for every $\log_2$ interval of 1.0 centered at integers. The three probe sets detecting *Olfr78* mRNA (arrows) confirmed the RNA-seq data (**a**, Fig. 1a, b, and Extended Data Table 1) showing *Olfr78* among the mRNAs most highly enriched in carotid body. Mouse CB *Olfr78* expression is consistent with previous microarray data[7,64]. **a-d**, *n*=3 cohorts of 10 animals each. Data as mean. **e**, Genomic locus showing the large cluster of ~160 Class I OR genes on chromosome 7, with region encoding MOR18 subfamily (*Olfr78*, *Olfr558*, and *Olfr557*) expanded below. We did not detect transcripts in either tissue for *Olfr557*, which lies adjacent to *Olfr558* in the cluster, or for the intervening (*Olfr33*, *Olfr559*) and intronic (*Olfr560*) ORs. Clusters of genes encoding globins, Trims, and USP proteins are also found with this OR cluster. Large box, coding sequence; arrowhead, coding orientation; small box, non-coding exons.
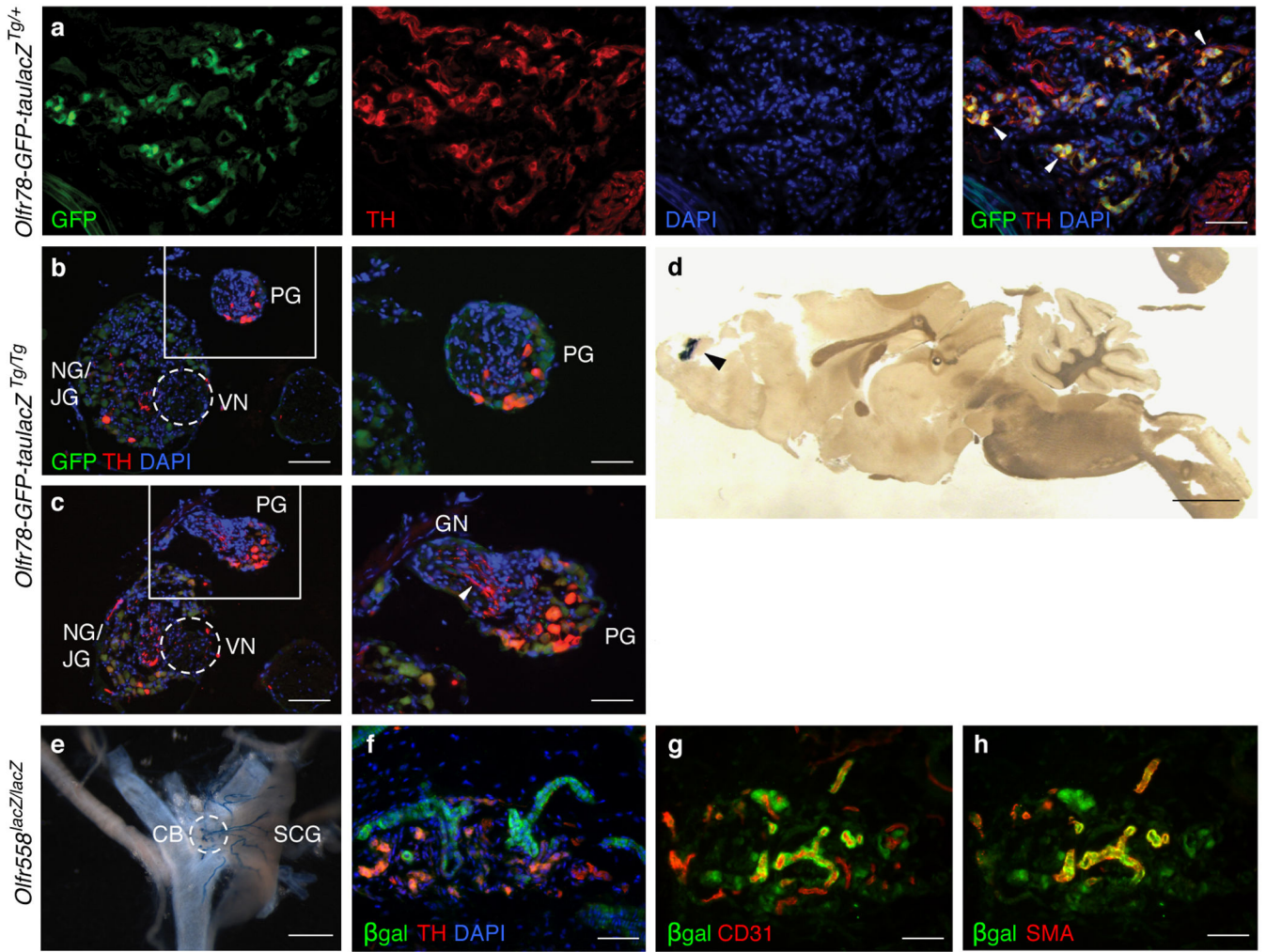
Extended Data Figure 3. *Olfr78* and *Olfr558* expression in tissues in the oxygen-sensing circuit
Expression of *Olfr78* reporter in heterozygous (**a**) and homozygous (**b-d**) *Olfr78-GFP-taulacZ* reporter animals[11]. **a-c**, Sections of carotid bifurcations stained for GFP (*Olfr78* reporter; green), tyrosine hydroxylase (TH; red), and DAPI (nuclei; blue). **a**, Section of CB showing co-expression of reporter GFP and TH in glomus cells. Monoallelic expression would predict that only half of TH-positive cells express the reporter[12]. Arrowheads, clusters of glomus cells expressing both GFP and TH. **b, c**, Sections of the same carotid bifurcation. Panels on right show close-ups of boxed region (petrosal ganglion, PG). No GFP-positive cells were found in petrosal ganglion. TH-positive nerve fibers (arrowheads) and cell bodies were found in glossopharyngeal nerve (GN) and petrosal ganglion. Dashed circle indicates vagus nerve (VN). NG/JG, nodose/jugular ganglia. **d**, X-gal staining of a brain sagittal section. Reporter expression (blue) was restricted to olfactory bulb (arrowhead) in this section and complete brain serial sagittal sections. Anterior, right; dorsal, up. **e-h**, *Olfr558* expression in a knockout/reporter mouse in which the *Olfr558* coding region is replaced with *lacZ* encoding β-galactosidase. **e**, *Olfr558* reporter expression in blood vessels of CB and SCG by X-gal staining. Heterozygous *Olfr558+/lacZ* samples showed the same pattern of staining (data not shown). **f-h**, CB sections immunostained for

β-galactosidase (*Olfr558* reporter; green), TH (red), with DAPI counterstain (blue) in **f**, and for β-galactosidase (green) and CD31 (red) in **g** or smooth muscle actin (red) in **h**. Scale bars, 100 μm (**a, b-right, c-right, f-h**), 200 μm (**b-left, c-left**), 500 μm (**e**), and 2 mm (**d**).
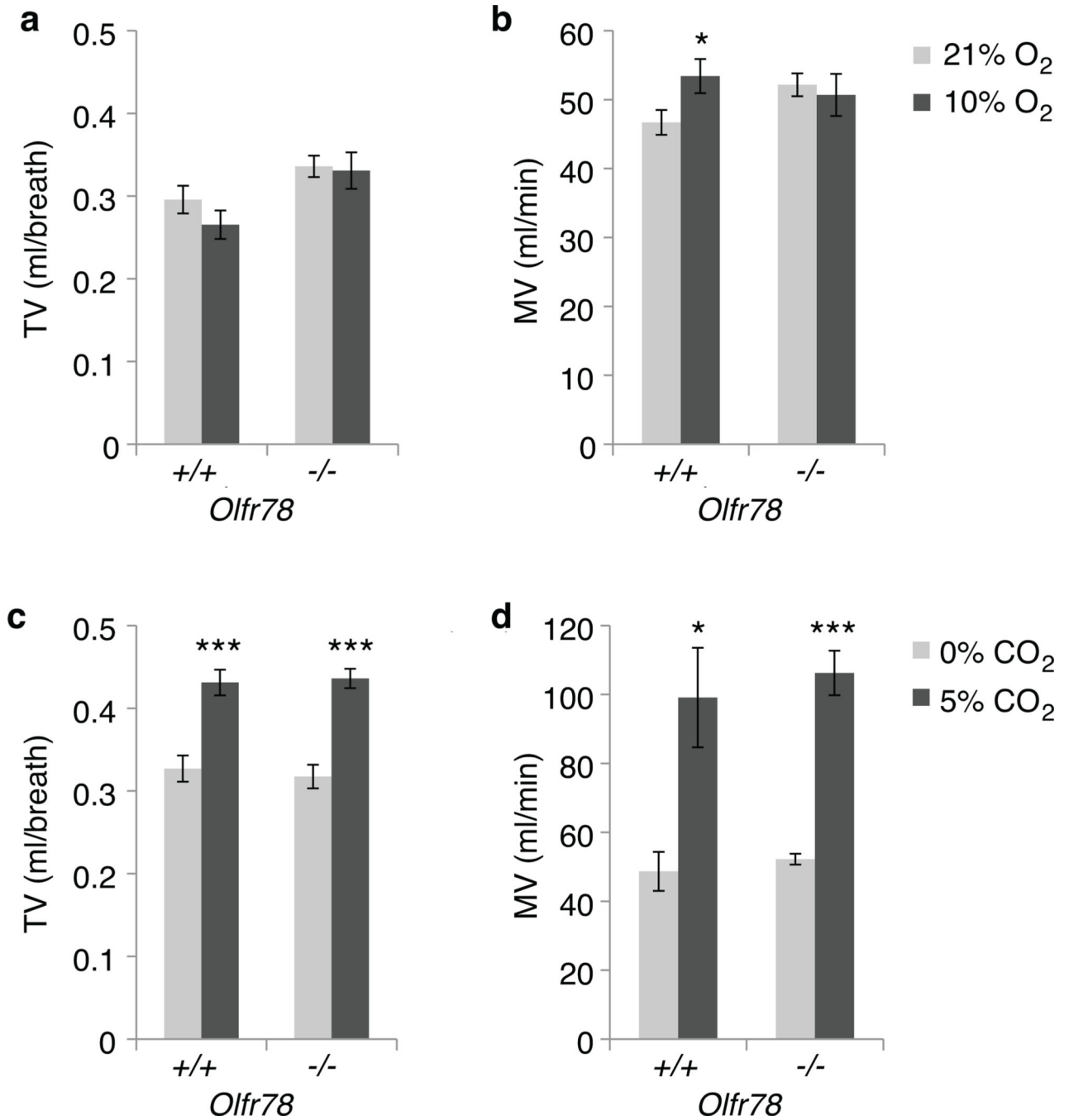
Extended Data Figure 4. Tidal volume and minute ventilation of *Olfr78*^{−/−} mutants exposed to hypoxia and hypercapnia

Whole body plethysmography of unrestrained, unanesthetized *Olfr78*^{+/+} control and *Olfr78*^{−/−} mutant littermates (as in Fig. 2). **a, b**, Tidal volume (TV) and minute ventilation (MV) of animals exposed to hypoxia. $n=9$ (+/+), 8 (−/−) animals. **c, d**, TV and MV of

animals exposed to hypercapnia. $n=4$ (+/+), 5 (−/−) animals. Data as mean ± s.e.m. *$P<0.05$, ***$P<0.001$ by paired t test.
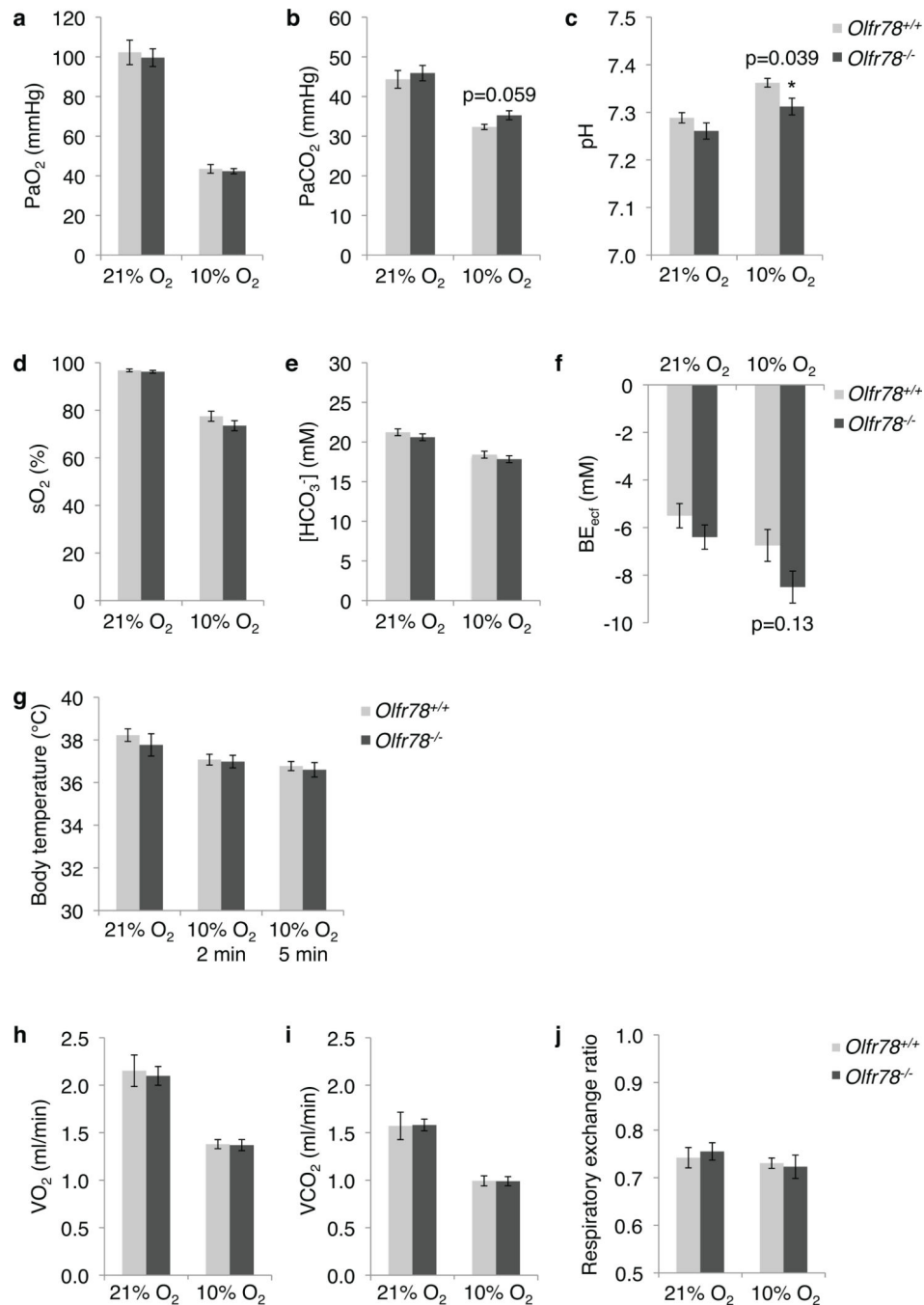
Extended Data Figure 5. Physiological responses of *Olfr78−/−* mutants to hypoxia *in vivo*
a-f, Arterial blood gas measurements of *Olfr78−/−* control and *Olfr78−/−* mutant animals exposed to hypoxia. PaO$_2$ (**a**), PaCO$_2$ (**b**), and pH (**c**) values of blood collected from the right carotid artery of anesthetized *Olfr78+/+* control and *Olfr78−/−* mutant animals exposed to normoxia (21% O$_2$) and hypoxia (10% O$_2$) for 3 min. Oxygen saturation (sO$_2$,**d**),

[HCO$_3^-$] (**e**), and base excess of extracellular fluid (BE$_{ecf}$,**f**) calculated from PaO$_2$ (**a**), PaCO$_2$ (**b**), and pH (**c**) values. *n*=4 (+/+, 21% O$_2$), 5 (−/−, 21% O$_2$), 4 (+/+, 10% O$_2$), 6 (−/−, 10% O$_2$) animals. **g**, Body temperature of unanesthetized *Olfr78*$^{+/+}$ control and *Olfr78*$^{-/-}$ mutant littermates in room air (21% O$_2$) and exposed to hypoxia (10% O$_2$) for indicated times. *n*=4 (+/+), 6 (−/−) animals. **h-j**, Metabolic values measured by indirect calorimetry of unanesthetized *Olfr78*$^{+/+}$ control and *Olfr78*$^{-/-}$ mutant littermates exposed to normoxia (21% O$_2$) and hypoxia (10% O$_2$) for 10 min. *n*=4 (+/+), 6 (−/−) animals. Data as mean ± s.e.m. *P<0.05 by unpaired *t* test.
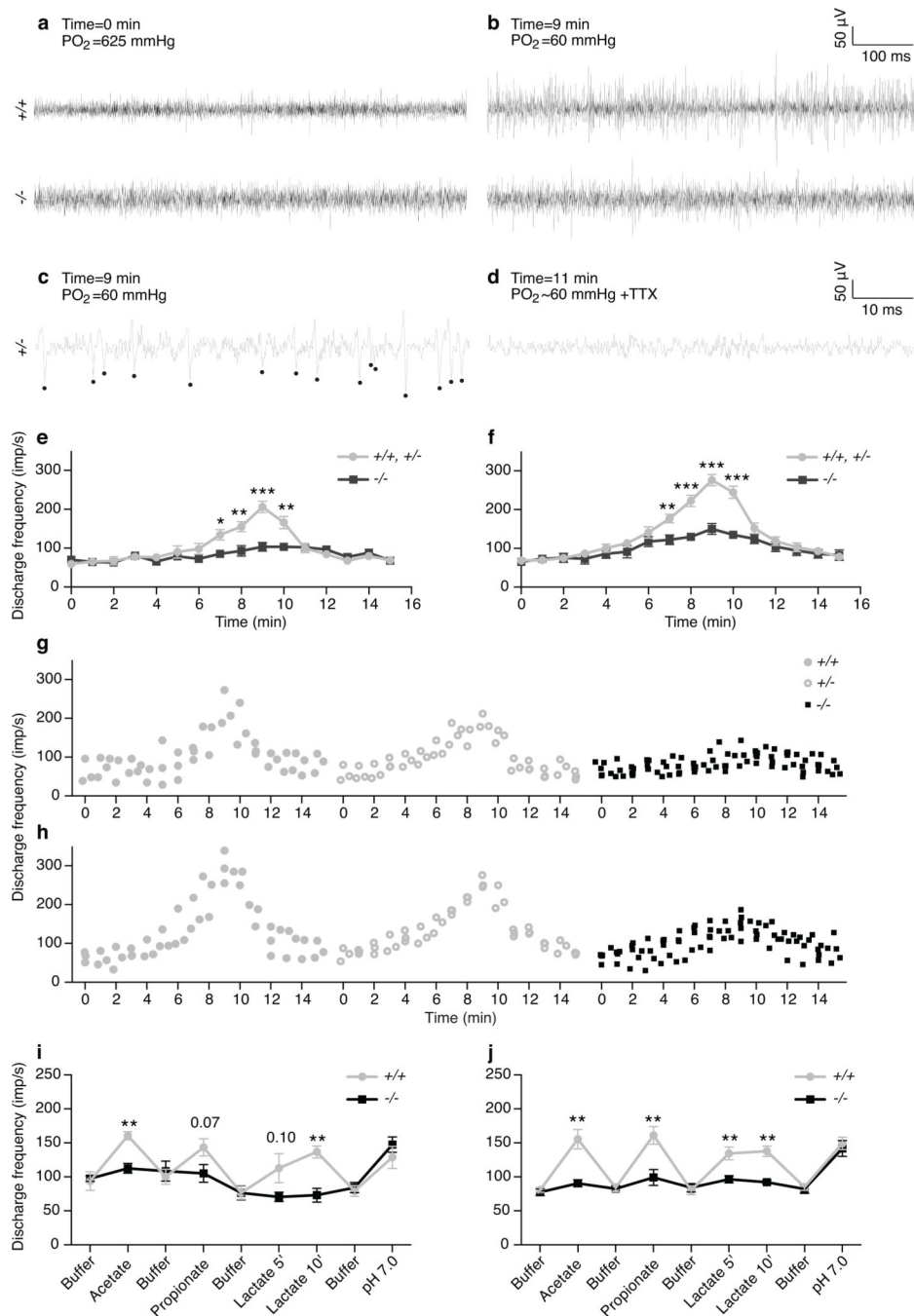
Extended Data Figure 6. Carotid body chemosensory responses assayed by carotid sinus nerve activity

a, b, Raw discharge frequency (extracellular recording) of carotid sinus nerves from *Olfr78*^{+/+} control and *Olfr78*^{−/−} mutant animals at time 0 (**a**) and 9 minutes (**b**) after the change in gas bubbling the perfusion buffer from 95% O_2/5% CO_2 to 95% N_2/5% CO_2. **c, d**, Carotid sinus nerve activity of an *Olfr78*^{+/−} nerve 9 minutes after the change in gas to 95% N_2/5% CO_2 (**c**) and 2 minutes later after addition of 7.5 μM tetrodotoxin (TTX) while still bubbling 95% N_2/5% CO_2 (**d**). Scored action potentials are marked by filled circles. **e-h**,

Time course of carotid sinus nerve activity in the *Olfr78* genotypes indicated scored using Spike2 software (**e, g**) or by hand (**f, h**) and showing mean ± s.e.m (**e, f**) or individual (**g, h**) values. The residual responses of *Olfr78*^{−/−} nerves to hypoxia were more apparent when scored by hand. $n=6$ (3 +/+, 3 +/−), 5 (−/−) animals. *$P<0.05$, **$P<0.01$, ***$P<0.001$ by unpaired t test. *Olfr78*^{+/+} and *Olfr78*^{+/−} recordings were not significantly different from each other at any time point, except for time=11 min, by unpaired t test ($P>0.05$). **i, j,** Time course of raw discharge of carotid sinus nerves from *Olfr78*^{+/+} control and *Olfr78*^{−/−} mutant animals in response to acetate (30 mM, 5 min), propionate (30 mM, 5 min), and lactate (30 mM, 5 and 10 min), and pH 7.0 (5 min) scored using Spike2 software (**i**) or by hand (**j**). Recovery times were 15 min between acetate, propionate, and lactate, and at least 30 min between lactate and pH 7.0. To minimize the contribution of endogenous hypoxic signals, the superperfusion buffer in the chamber was maintained at hyperoxic conditions ($PO_2=625$ mmHg). $n=5$ (+/+), 5 (−/−) animals. Data as mean ± s.e.m. *$P<0.05$, **$P<0.01$ by unpaired t test.

Chemical	EC$_{50}$ (mM)	95% CI	Relative Max
Sodium acetate	2.01	1.69-2.41	0.99
Sodium propionate	0.63	0.49-0.82	0.69
Sodium lactate	4.04	2.59-6.30	0.34
Sodium chloride	ND	ND	ND
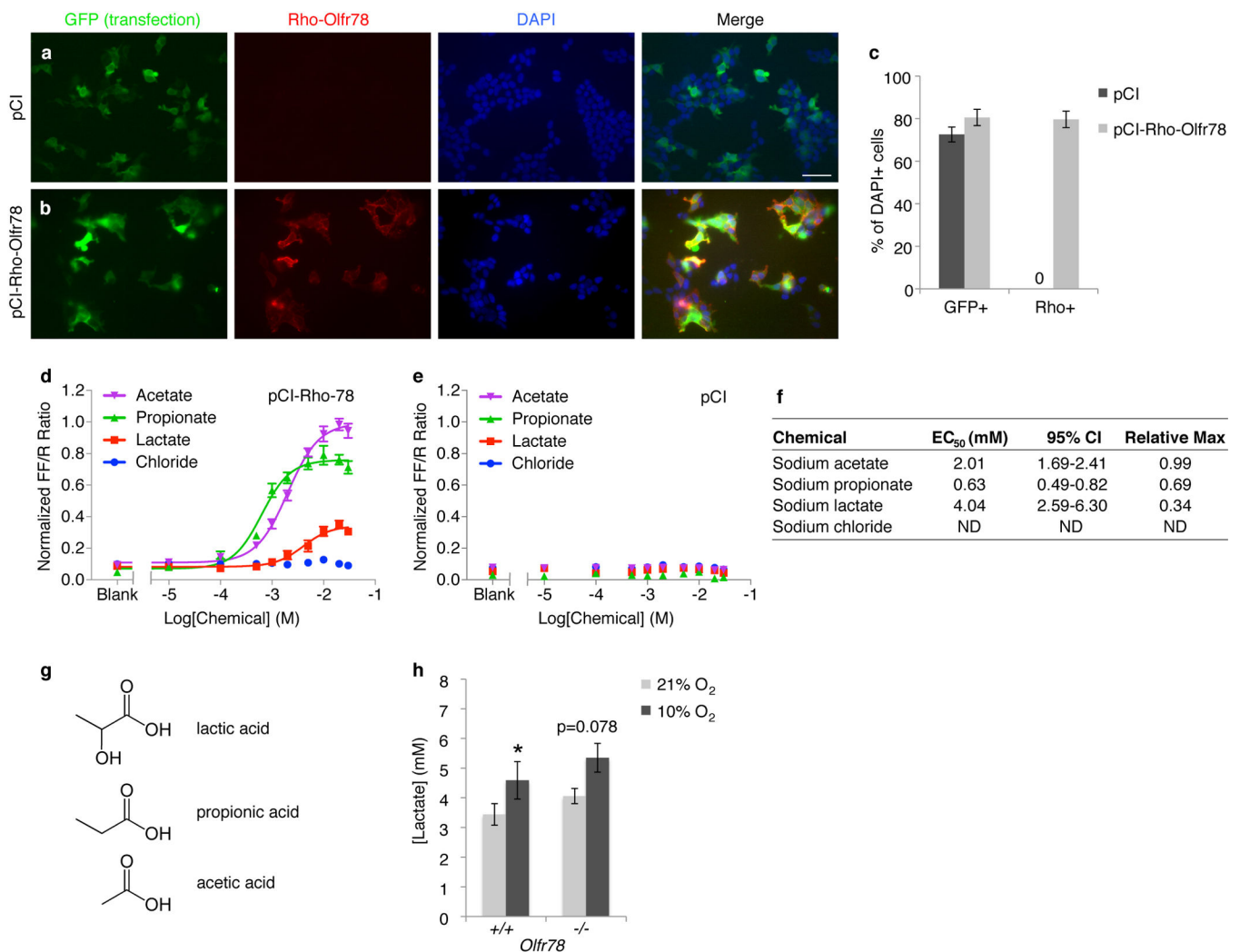
Extended Data Figure 7. Lactate activates Olfr78 expressed in HEK293T cells and increases acutely in blood in hypoxia *in vivo*

a, b, HEK293T cells transfected with empty vector pCI (**a**) or pCI-Rho-Olfr78 (**b**) and RTP1S (OR transport protein) and cytoplasmic GFP (co-transfection marker) plasmids. Transfected cells were stained before fixation to detect Rho-tagged Olfr78 (anti-Rho; red) on the cell surface. GFP (transfection marker, green); DAPI (nuclei, blue). Bar, 100 μm. **c**, Quantitation of cells expressing GFP and Rho as percentage of DAPI-positive cells in fields shown in **a** and **b**. n=164 (pCI), 108 (pCI-Rho-Olfr78) cells. Data as percent ± standard error of percentage. **d**, Dose-response curves for propionate, acetate, and chloride compared to lactate in activation of Olfr78 in transfected HEK293T cells as in Fig. 4a. n=8 (propionate), 12 (acetate), 4 (chloride), and 12 (lactate) wells. Data as mean ± s.e.m. By analysis of variance (ANOVA), all chemicals except chloride (P=0.309) showed significant difference (P<0.001). **e**, Dose-response curves as in **c** except cells were transfected with empty vector (pCI). ANOVA showed no significant difference (P>0.05) for any chemical. **f**, EC_{50}, 95% confidence interval of EC_{50}, and relative maximal activation values from fitted curves in **c**. ND, not determined due to lack of curve fitting to data. **g**, Structures of the short-chain fatty acids. **h**, Lactate concentrations in blood collected from tail artery of restrained, unanesthetized $Olfr78^{+/+}$ control and $Olfr78^{-/-}$ mutant littermates exposed to hypoxia (10% O_2) for 4–5 min. Values for animals in normoxia (21% O_2) are likely to be an overestimate of baseline concentrations due to greater restraint required to immobilize animals in normoxia[41]. n=5 (+/+), 6 (−/−) animals. Data as mean ± s.e.m. *P<0.05 by paired t test.
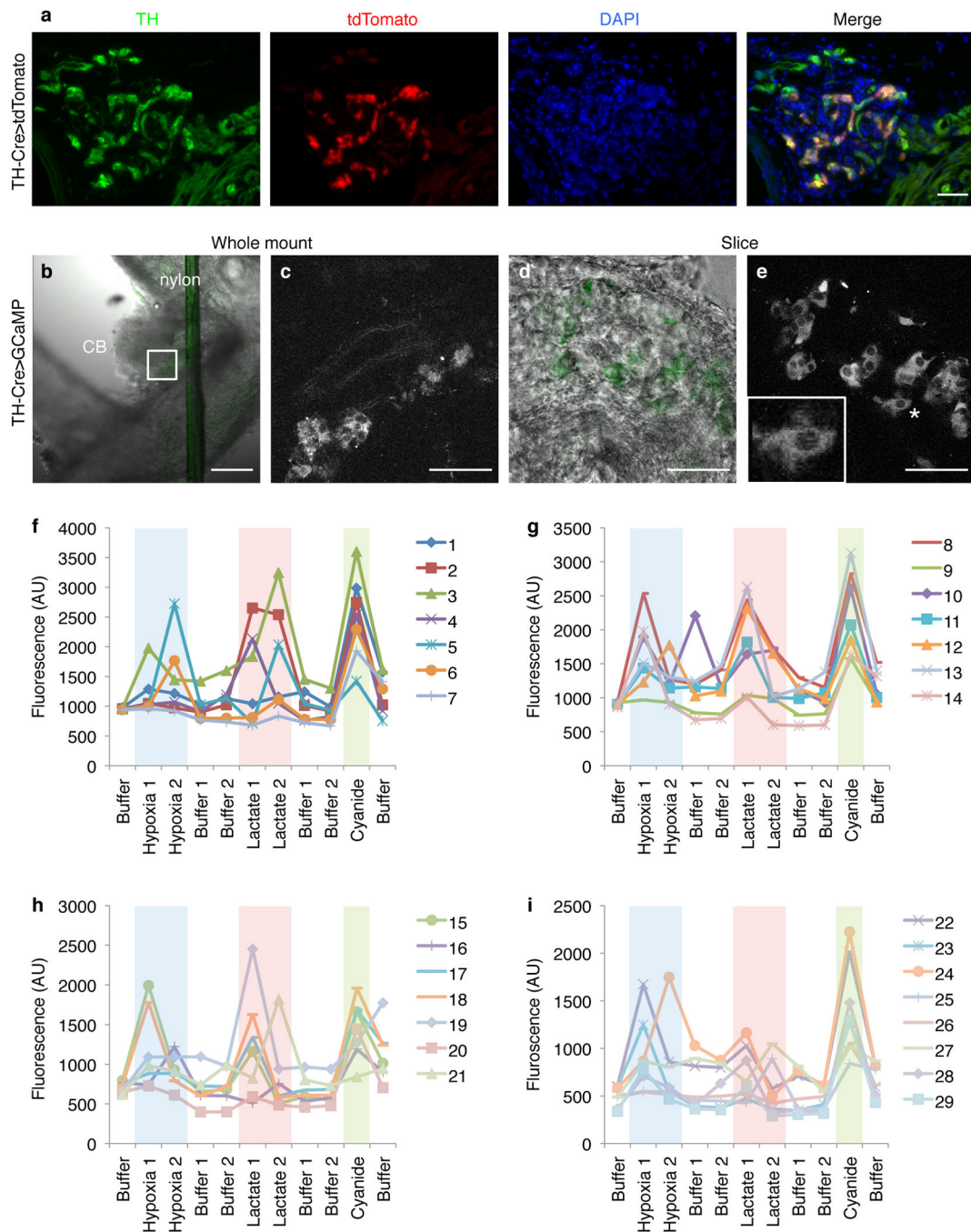
Extended Data Figure 8. Calcium imaging of responses of carotid body glomus cells to chemosensory stimuli

a, Carotid body (CB) of a *Th-Cre; ROSA-tdTomato* adult immunostained for the Cre-dependent reporter tdTomato (red) and TH (green) to show glomus cells[31,32,34] and counterstained with DAPI (nuclei, blue). tdTomato labeled glomus cells. **b-e**, Tissue preparations for calcium imaging of CBs from *TH-Cre; ROSA-GCaMP3* animals that express the calcium indicator GCaMP3 selectively in glomus cells[31–33]. **b**, DIC image of whole mount carotid bifurcation with GCaMP3 fluorescence pseudocolored green. **c**, High

magnification, two-photon image of boxed region in **b. d**, DIC image of CB tissue slice with GCaMP3 fluorescence pseudocolored green. **e**, Two-photon image of CB slice in **d**. Inset shows glomus cell marked by asterisk at higher magnification. GCaMP3 fluorescence was seen in cytoplasm and excluded from nucleus of glomus cells. Bars, 100 μm (**a**), 200 μm (**b**), 50 μm (**c-e**). **f-i** Time course of calcium responses of individual glomus cells to hypoxia, lactate, and cyanide. Whole mount CBs were exposed sequentially to hypoxia (40–50 mmHg), lactate (30 mM), and cyanide (2 mM). Interval between data points is ~2 minutes, the time required to acquire a stack of images through the CB, excluding the 2 minute ramp times between stimuli. All glomus cells analyzed (*n*=42 cells) responded strongly to cyanide. Fluorescence traces shown are the 29 individual glomus cells that responded to both hypoxia and lactate, arranged in order of decreasing initial fluorescence intensity. The other 13 glomus cells responded to either hypoxia (9 cells) or lactate (4 cells). Multiple data points for buffer or stimuli were averaged to generate the data presented in Fig. 4c. Background colors match bar colors in Fig. 4d.

Extended Data Table 1

Top 150 genes highly expressed in carotid body vs. adrenal medulla by RNA-seq.

Gene Name	CB*	AM*	CB/AM†	Comment	Gene Name	CB*	AM*	CB/AM†	Comment
Cpne4	9.9	0.4	9.4	Ca+2-dep membrane binding	Cpa3	9.4	3.7	5.7	Peptidase, mast cell
Slc9a2	9.2	0.3	8.9	Na+/K+ exchanger	Dlx6	5.7	0.0	5.7	Hox TF, brain
Coch	10.1	1.2	8.9	Expressed in ear cells	2210407C18Rik	5.2	−0.6	5.7	
Abcc2	9.0	0.6	8.4	ABC transporter	Cwh43	7.0	1.3	5.7	GPI-anchor lipid remodeling
Barx1	7.7	−0.6	8.3	Hox TF, neural crest	Cma1	9.8	4.2	5.7	Chymase, mast cell
Higd1c	11.3	3.2	8.1	Membrane protein	Nmu	5.0	−0.6	5.6	Neuropeptide, neuromedin U
Hmx3	7.3	−0.6	7.8	Hox TF, ear and neurons	Drd1a	5.8	0.3	5.5	GPCR, dopamine receptor 1a
Hmx2	7.6	−0.2	7.8	Hox TF, ear	Sfrp4	9.8	4.3	5.5	Secreted frizzled
Ccl21a	8.2	0.4	7.8	Chemokine	Bcl11b	8.6	3.1	5.5	Tumor suppressor
AB099516	13.4	5.6	7.8	Methyltransferase-like	Myh11	10.6	5.1	5.5	Smooth muscle myosin
Pcolce2	11.3	3.6	7.6	Procollagen peptidase enhancer	Ptx4	4.9	−0.6	5.5	Multifunctional conserved
Lypd2	8.3	0.7	7.5	LY6/PLAUR domain containing	Rxrg	8.7	3.3	5.5	Retinoid X receptor, nuclear
Gkn3	8.7	1.3	7.3	Pseudogene	Pax8	4.9	−0.6	5.5	Paired box TF, thyroid
Mcpt4	8.8	1.4	7.3	Mast cell proliferation	Crhr1	5.7	0.3	5.4	GPCR, hormone
Gm21541	7.3	0.0	7.3	Chemokine	Gm694	4.9	−0.6	5.4	
Ccl21b	7.3	0.0	7.3	Chemokine	Mc4r	7.5	2.1	5.4	GPCR, melanocortin receptor
Gm13304	7.4	0.1	7.3	Chemokine	Sgca	5.3	0.0	5.4	Extracellular matrix
Tpsb2	7.8	0.6	7.1	Tryptase, mast cell	Gm9885	5.4	0.1	5.3	
Cpne5	8.1	1.0	7.1	Ca+2-dep membrane binding	Kcna1	12.4	7.1	5.3	Voltage-gated K− channel, K_v 1.1
H19	8.7	1.7	7.1	Maternal imprinted	Smim5	8.0	2.7	5.3	Integral membrane protein
Gm10768	7.1	0.1	7.0		Ccl11	9.0	3.8	5.3	Chemokine
Gm1987	8.2	1.3	6.9	Chemokine	Pllp	6.6	1.3	5.2	Involved in myelination
LOC100041504	7.2	0.3	6.9	Chemokine	Galnt9	8.8	3.6	5.2	GalNac transferase
Cst12	6.6	−0.2	6.9	Cysteine endopeptidase	C1qtnf9	6.9	1.7	5.2	Adipokine
Vit	9.3	2.4	6.9	Extracellular matrix	Hcn1	6.6	1.4	5.2	Hyperpol, CNG K+ channel
Mpz	9.0	2.1	6.8	Myelin	Prss12	6.8	1.6	5.2	Trypsin, neuronal plasticity
Ccl21c	7.2	0.4	6.8	Chemokine	Rergl	6.1	0.9	5.2	Putative GTPase
Prdm6	6.3	−0.6	6.8	Histone methyltransferase	4931429I11Rik	6.3	1.1	5.2	

Gene Name	CB*	AM*	CB/AM†	Comment	Gene Name	CB*	AM*	CB/AM†	Comment
Susd5	8.1	1.3	6.8	Sushi domain containing	Enpp3	6.8	1.6	5.2	Nucleotide ectoenzyme
Rxfp1	6.6	-0.2	6.8	GPCR, relaxin receptor	Saa1	5.3	0.1	5.2	Serum amyloid
Cytl1	10.1	3.3	6.8	Cytokine-like	Itgb4	9.3	4.2	5.1	Integrin
Olfr558	8.5	1.8	6.8	GPCR, olfactory receptor	Cpn1	4.5	-0.6	5.1	Carboxypeptidase
Ly6h	11.1	4.4	6.8	Lymphocyte antigen complex	Cspg4	9.6	4.6	5.0	Extracellular matrix proteoglycan
Gpr139	6.2	-0.6	6.7	GPCR	9130206I24Rik	7.2	2.2	5.0	
C530044C16Rik	7.7	1.0	6.7		Areg	4.4	-0.6	5.0	EGF/TGF-α homolog, glia
Olfr78	11.7	5.1	6.7	GPCR, olfactory receptor	Trabd2b	8.9	3.9	5.0	Neg regulator of Wnt signaling
Sfrp2	10.3	3.6	6.6	Secreted frizzled-related	Chrdl1	9.1	4.2	5.0	BMP4 antagonist, neuron
Pin	9.4	2.7	6.6	Ca+2-ATPase inhibitor, heart	Ltbp2	7.3	2.4	5.0	Extracellular matrix
Tph1	7.4	0.7	6.6	Serotonin biosynthesis	Rbp7	7.0	2.1	4.9	Retinol binding protein
Gm10591	7.3	0.6	6.6	Chemokine	Mmm1	7.9	3.0	4.9	Carrier of platelet proteins
Cntnap4	6.0	-0.6	6.5	Neural cell adhesion	Hrk	8.0	3.1	4.9	Promotes apoptosis
LOC100041593	7.3	0.8	6.5		Ptgfr	6.8	1.9	4.9	GPCR, prostaglandin receptor
Thbs4	7.3	0.8	6.5	Cell adhesion glycoprotein	Tpsab1	5.0	0.1	4.9	Tryptase
Tnmd	6.3	-0.2	6.5	Cartilage-specific glycoprotein	Pthlh	7.7	2.9	4.9	Parathyroid hormone-like
Gpr20	7.1	0.6	6.5	GPCR	Fndc1	8.9	4.0	4.9	Fibronectin domain containing
Cntn5	5.9	-0.6	6.5	Neural cell adhesion	Bmx	6.6	1.8	4.8	Non-receptor tyrosine kinase
Dgkh	11.2	4.8	6.4	Diacylglycerol kinase	Car12	8.7	3.9	4.8	Carbonic anydrase, extracellular
Xirp1	5.9	-0.6	6.4	Actin binding	Atp8b1	7.0	2.2	4.8	Cation transport ATPase
Ptx3	7.1	0.8	6.4	Innate immunity, inflammation	Cd163l1	4.6	-0.2	4.8	Scavenger receptor; immune
Prom1	9.1	2.7	6.4	Adult stem cell maintenance	Gcsam	5.4	0.6	4.8	PDZ domain containing
Nov	9.2	2.8	6.4	Extracellular matrix, cancer	Acta2	13.9	9.1	4.8	Smooth muscle actin, aorta
Adamtsl3	6.9	0.6	6.3	Metalloprotease, cancer	Dcn	15.1	10.3	4.8	Extracellular matrix proteoglycan
Gdnf	7.1	0.7	6.3	Glial derived neurotrophic factor	Dlx6as1	7.2	2.4	4.8	Noncoding RNA, GABA neurons
Dlx5	7.5	1.3	6.3	Hox TF, bone	Chp2	6.9	2.2	4.7	Ca+2-binding, pH control
Inmt	11.8	5.7	6.2	Indolethylamine N-methylase	Gm10808	5.2	0.4	4.7	
Mfap5	11.5	5.4	6.1	Microfibril-associated glycoprotein	Col8a1	10.1	5.4	4.7	Collagen
Scara3	9.4	3.3	6.1	ROS scavenger	Foxd1	6.0	1.3	4.7	Forkhead TF
Pgf	10.0	3.9	6.0	Placental growth factor	Igfbp4	13.2	8.5	4.7	Insulin-like growth factor binding
Mustn1	10.0	4.0	6.0	Expressed in muscle and bone	Alpl	8.5	3.8	4.7	Alkaline phosphatase

Gene Name	CB*	AM*	CB/AM†	Comment	Gene Name	CB*	AM*	CB/AM†	Comment
Pkib	12.5	6.5	6.0	cAMP-dep kinase inhibitor	Dhrs2	6.2	1.5	4.7	Dehydrogenase/reductase
Comp	6.6	0.6	6.0	Cartilage matrix	Lmod3	4.5	-0.2	4.7	Expressed in muscle
Gap43	12.3	6.3	6.0	Neuronal growth cone	Rnase1	5.1	0.4	4.7	Secretory RNase
Shisa3	8.7	2.7	6.0	Fgf and Wnt signaling interactor	Gm15998	4.4	-0.2	4.7	
Cma2	5.4	-0.6	6.0	Chymase, mast cell	Cnn1	7.4	2.7	4.7	Thin filament associated, muscle
Gjb5	6.1	0.1	6.0	Gap junction	Col2a1	4.1	-0.6	4.7	Collagen
Meox2	9.1	3.2	5.9	Hox TF, mesenchyme	Osr1	8.2	3.6	4.7	TF, odd-skipped related
Plch1	5.7	-0.2	5.9	Phospholipase	Hepacam2	6.0	1.3	4.6	Centrosome maturation
Tlx1	5.3	-0.6	5.9	Hox TF-spleen, neurons, T cells	Fcer1a	5.1	0.5	4.6	IgE receptor, Fc
Igfbp6	12.1	6.3	5.8	Insulin-binding protein	Pax9	4.1	-0.6	4.6	Paired box TF
Rgs5	14.9	9.0	5.8	GTPase activator	Ncmap	7.5	2.8	4.6	Myelin-associated
Edn1	8.0	2.2	5.8	Endothelin 1, vasoconstrictor	Plsl	5.5	0.8	4.6	Plastins, hematopoietic cells
Rspo1	10.1	4.2	5.8	Activator of Wnt signaling	Fbln7	11.1	6.5	4.6	Extracellular matrix adhesion
Upb1	7.0	1.2	5.8	Pyrimidine degradation	Folr2	8.4	3.8	4.6	Folate receptor
Scnn1b	9.4	3.6	5.8	ENaC Na+ channel, beta subunit	Msx1	6.9	2.3	4.6	Hox, craniofacial
Fgf7	6.6	0.8	5.8	Fibroblast growth factor	Tmem158	12.7	8.1	4.6	Peptide receptor

*
CB and AM values are log2(aligned reads per 10⁷ reads) as in Extended Data Fig. 2a.

†
Log2(CB/AM) ratios as in Extended Data Fig. 1a. All genes were significantly different between CB and AM by paired *t* test ($P<0.05$), except Bmx ($P=0.056$). Yellow highlight, genes for olfactory receptors. Blue highlight, genes previously shown to be expressed in CB (ref[40,65,66]). TF, transcription factor; GPCR, G protein-coupled receptor; ROS, reactive oxygen species; CNG, cyclic nucleotide-gated.

Extended Data Table 2

Expression of genes associated with olfactory neurons.

Gene Name	Function	RPKM		
		CB*	AM*	CB/AM
Olfr78	olfactory receptor	101	1.1	92 †
Olfr558	olfactory receptor	13	0.13	102 ‡
Gnal	G protein, alpha subunit	11	3.9	2.8 †
Adcy3	adenylate cyclase	3.2	5.2	0.61 †
Cnga2	cyclic nucleotide-gated channel	0.060	0.10	0.61
Cnga4	cyclic nucleotide-gated channel	0.075	0.053	1.4
Cngb1	cyclic nucleotide-gated channel	0.23	0.23	1.0
Ano2	calcium-activated chloride channel	0.75	0.11	6.8 †
Ric8b	guanine nucleotide exchange factor	8.6	8.8	1.0
Rtp1	olfactory receptor trafficking	0.082	0.11	0.77
Rtp2	olfactory receptor trafficking	0.048	0.047	1.0
Reep1	olfactory receptor trafficking	6.2	4.3	1.4
Omp	mature olfactory neuron marker	4.0	3.5	1.1

* Carotid body (CB) and adrenal medulla (AM) values are reads per kilobase per million (RPKM) normalized to longest mRNA isoform for each gene.

† $P<0.05$ and

‡ $P<0.01$ between CB and AM by paired t test.

Supplementary Material

Refer to Web version on PubMed Central for supplementary material.

Acknowledgments

References

1. Semenza GL. Hypoxia-inducible factors in physiology and medicine. Cell. 2012; 148:399–408. [PubMed: 22304911]

2. Kumar P, Prabhakar NR. Peripheral chemoreceptors: function and plasticity of the carotid body. Compr Physiol. 2012; 2:141–219. [PubMed: 23728973]

3. Lee LY, Morton RF, Lundberg JM. Pulmonary chemoreflexes elicited by intravenous injection of lactic acid in anesthetized rats. J Appl Physiol (1985). 1996; 81:2349–2357. [PubMed: 9018478]

4. Hardarson T, Skarphedinsson JO, Sveinsson T. Importance of the lactate anion in control of breathing. J Appl Physiol (1985). 1998; 84:411–416. [PubMed: 9475845]

5. Kirsch JR, D'Alecy LG. Role of tissue lactate and substrate availability in 1,3-butanediol-enhanced hypoxic survival in the mouse. Stroke. 1983; 14:971–976. [PubMed: 6362095]

6. Marina N, et al. Brainstem hypoxia contributes to the development of hypertension in the spontaneously hypertensive rat. Hypertension. 2015; 65:775–783. [PubMed: 25712724]

7. Ganfornina MD, et al. Comparative gene expression profile of mouse carotid body and adrenal medulla under physiological hypoxia. J Physiol. 2005; 566:491–503. [PubMed: 15890701]

8. Fleischer J, Breer H, Strotmann J. Mammalian olfactory receptors. Front Cell Neurosci. 2009; 3:9. [PubMed: 19753143]

9. Flegel C, Manteniotis S, Osthold S, Hatt H, Gisselmann G. Expression profile of ectopic olfactory receptors determined by deep sequencing. PLoS One. 2013; 8:e55368. [PubMed: 23405139]

10. Kang N, Koo J. Olfactory receptors in non-chemosensory tissues. BMB Rep. 2012; 45:612–622. [PubMed: 23186999]

11. Conzelmann S, et al. A novel brain receptor is expressed in a distinct population of olfactory sensory neurons. Eur J Neurosci. 2000; 12:3926–3934. [PubMed: 11069588]

12. Chess A, Simon I, Cedar H, Axel R. Allelic inactivation regulates olfactory receptor gene expression. Cell. 1994; 78:823–834. [PubMed: 8087849]

13. Weber M, Pehl U, Breer H, Strotmann J. Olfactory receptor expressed in ganglia of the autonomic nervous system. J Neurosci Res. 2002; 68:176–184. [PubMed: 11948663]

14. Pluznick JL, et al. Olfactory receptor responding to gut microbiota-derived signals plays a role in renin secretion and blood pressure regulation. Proc Natl Acad Sci U S A. 2013; 110:4410–4415. [PubMed: 23401498]

15. Matsuura S. Chemoreceptor properties of glomus tissue found in the carotid region of the cat. J Physiol. 1973; 235:57–73. [PubMed: 4778142]

16. Bozza T, et al. Mapping of class I and class II odorant receptors to glomerular domains by two distinct types of olfactory sensory neurons in the mouse. Neuron. 2009; 61:220–233. [PubMed: 19186165]

17. Gautier H. Interactions among metabolic rate, hypoxia, and control of breathing. J Appl Physiol (1985). 1996; 81:521–527. [PubMed: 8872614]

18. Shirahata M, Kostuk EW, Pichard LE. Carotid chemoreceptor development in mice. Respir Physiol Neurobiol. 2013; 185:20–29. [PubMed: 22634368]

19. Saito H, Chi Q, Zhuang H, Matsunami H, Mainland JD. Odor coding by a Mammalian receptor repertoire. Sci Signal. 2009; 2:ra9. [PubMed: 19261596]

20. Remesy C, Demigne C, Chartier F. Origin and utilization of volatile fatty acids in the rat. Reprod Nutr Dev. 1980; 20:1339–1349. [PubMed: 7349486]

21. Wolever TM, Josse RG, Leiter LA, Chiasson JL. Time of day and glucose tolerance status affect serum short-chain fatty acid concentrations in humans. Metabolism. 1997; 46:805–811. [PubMed: 9225836]

22. Knowles SE, Jarrett IG, Filsell OH, Ballard FJ. Production and utilization of acetate in mammals. Biochem J. 1974; 142:401–411. [PubMed: 4441381]

23. Buckler KJ, Turner PJ. Oxygen sensitivity of mitochondrial function in rat arterial chemoreceptor cells. J Physiol. 2013; 591:3549–3563. [PubMed: 23671162]

24. Monti-Bloch L, Abudara V, Eyzaguirre C. Electrical communication between glomus cells of the rat carotid body. Brain Res. 1993; 622:119–131. [PubMed: 7902188]

25. Pokorski M, Lahiri S. Aortic and carotid chemoreceptor responses to metabolic acidosis in the cat. Am J Physiol. 1983; 244:R652–R658. [PubMed: 6846573]

26. Rigual R, Lopez-Lopez JR, Gonzalez C. Release of dopamine and chemoreceptor discharge induced by low pH and high PCO2 stimulation of the cat carotid body. J Physiol. 1991; 433:519–531. [PubMed: 1841956]

27. Huckabee WE. Relationships of pyruvate and lactate during anaerobic metabolism. III. Effect of breathing low-oxygen gases. J Clin Invest. 1958; 37:264–271. [PubMed: 13513757]

28. Tan ZY, et al. Acid-sensing ion channels contribute to transduction of extracellular acidosis in rat carotid body glomus cells. Circ Res. 2007; 101:1009–1019. [PubMed: 17872465]

29. Buckler KJ. TASK channels in arterial chemoreceptors and their role in oxygen and acid sensing. Pflugers Arch. 2015; 467:1013–1025. [PubMed: 25623783]

30. van der Schier R, Roozekrans M, van Velzen M, Dahan A, Niesters M. Opioid-induced respiratory depression: reversal by non-opioid drugs. F1000Prime Rep. 2014; 6:79. [PubMed: 25343036]

Methods and Extended Data References

31. Gong S, et al. Targeting Cre recombinase to specific neuron populations with bacterial artificial chromosome constructs. J Neurosci. 2007; 27:9817–9823. [PubMed: 17855595]

32. Lindeberg J, et al. Transgenic expression of Cre recombinase from the tyrosine hydroxylase locus. Genesis. 2004; 40:67–73. [PubMed: 15452869]

33. Zariwala HA, et al. A Cre-dependent GCaMP3 reporter mouse for neuronal imaging in vivo. J Neurosci. 2012; 32:3131–3141. [PubMed: 22378886]

34. Madisen L, et al. A robust and high-throughput Cre reporting and characterization system for the whole mouse brain. Nat Neurosci. 2010; 13:133–140. [PubMed: 20023653]

35. Kumar ME, et al. Mesenchymal cells. Defining a mesenchymal progenitor niche at single-cell resolution. Science. 2014; 346:1258810. [PubMed: 25395543]

36. Drorbaugh JE, Fenn WO. A barometric method for measuring ventilation in newborn infants. Pediatrics. 1955; 16:81–87. [PubMed: 14394741]

37. Peng YJ, et al. H2S mediates O2 sensing in the carotid body. Proc Natl Acad Sci U S A. 2010; 107:10719–10724. [PubMed: 20556885]

38. Trapp S, Tucker SJ, Gourine AV. Respiratory responses to hypercapnia and hypoxia in mice with genetic ablation of Kir5.1 (Kcnj16). Exp Physiol. 2011; 96:451–459. [PubMed: 21239463]

39. Kline DD, Peng YJ, Manalo DJ, Semenza GL, Prabhakar NR. Defective carotid body function and impaired ventilatory responses to chronic hypoxia in mice partially deficient for hypoxia-inducible factor 1 alpha. Proc Natl Acad Sci U S A. 2002; 99:821–826. [PubMed: 11792862]

40. Kline DD, et al. Kv1.1 deletion augments the afferent hypoxic chemosensory pathway and respiration. J Neurosci. 2005; 25:3389–3399. [PubMed: 15800194]

41. Balcombe JP, Barnard ND, Sandusky C. Laboratory routines cause animal stress. Contemp Top Lab Anim Sci. 2004; 43:42–51. [PubMed: 15669134]

42. Zhuang H, Matsunami H. Evaluating cell-surface expression and measuring activation of mammalian odorant receptors in heterologous cells. Nat Protoc. 2008; 3:1402–1413. [PubMed: 18772867]

43. Piskuric NA, Nurse CA. Effects of chemostimuli on [Ca2+]i responses of rat aortic body type I cells and endogenous local neurons: comparison with carotid body cells. J Physiol. 2012; 590:2121–2135. [PubMed: 22431340]

44. Pardal R, Ludewig U, Garcia-Hirschfeld J, Lopez-Barneo J. Secretory responses of intact glomus cells in thin slices of rat carotid body to hypoxia and tetraethylammonium. Proc Natl Acad Sci U S A. 2000; 97:2361–2366. [PubMed: 10681419]

45. Pardal R, Ortega-Saenz P, Duran R, Lopez-Barneo J. Glia-like stem cells sustain physiologic neurogenesis in the adult mammalian carotid body. Cell. 2007; 131:364–377. [PubMed: 17956736]

46. Gourine AV. On the peripheral and central chemoreception and control of breathing: an emerging role of ATP. J Physiol. 2005; 568:715–724. [PubMed: 16141266]

47. Anichkov, SV.; Belenk'ii, ML. Pharmacology of the Carotid Body Chemoreceptors. Pergamon Press; 1963.

48. Lopez-Barneo J, Lopez-Lopez JR, Urena J, Gonzalez C. Chemotransduction in the carotid body: K + current modulated by PO2 in type I chemoreceptor cells. Science. 1988; 241:580–582. [PubMed: 2456613]

49. Buckler KJ. A novel oxygen-sensitive potassium current in rat carotid body type I cells. J Physiol. 1997; 498(Pt 3):649–662. [PubMed: 9051577]

50. Williams SE, et al. Hemoxygenase-2 is an oxygen sensor for a calcium-sensitive potassium channel. Science. 2004; 306:2093–2097. [PubMed: 15528406]

51. Wyatt CN, et al. AMP-activated protein kinase mediates carotid body excitation by hypoxia. J Biol Chem. 2007; 282:8092–8098. [PubMed: 17179156]

52. Streller T, Huckstorf C, Pfeiffer C, Acker H. Unusual cytochrome a592 with low PO2 affinity correlates as putative oxygen sensor with rat carotid body chemoreceptor discharge. FASEB J. 2002; 16:1277–1279. [PubMed: 12153998]

53. Mills E, Jobsis FF. Mitochondrial respiratory chain of carotid body and chemoreceptor response to changes in oxygen tension. J Neurophysiol. 1972; 35:405–428. [PubMed: 4338562]

54. Wilson DF, et al. The primary oxygen sensor of the cat carotid body is cytochrome a3 of the mitochondrial respiratory chain. FEBS Lett. 1994; 351:370–374. [PubMed: 8082798]

55. Quintana A, et al. Fatal breathing dysfunction in a mouse model of Leigh syndrome. J Clin Invest. 2012; 122

56. Stettner GM, Viscomi C, Zeviani M, Wilichowski E, Dutschmann M. Hypoxic and hypercapnic challenges unveil respiratory vulnerability of Surf1 knockout mice, an animal model of Leigh syndrome. Mitochondrion. 2011; 11:413–420. [PubMed: 21167962]

57. Pronicka E, et al. Compulsory hyperventilation and hypocapnia of patients with Leigh syndrome associated with SURF1 gene mutations as a cause of low serum bicarbonates. J Inherit Metab Dis. 2001; 24:707–714. [PubMed: 11804207]

58. Piruat JI, Pintado CO, Ortega-Saenz P, Roche M, Lopez-Barneo J. The mitochondrial SDHD gene is required for early embryogenesis, and its partial deficiency results in persistent carotid body glomus cell activation with full responsiveness to hypoxia. Mol Cell Biol. 2004; 24:10933–10940. [PubMed: 15572694]

59. Mulligan E, Lahiri S, Storey BT. Carotid body O2 chemoreception and mitochondrial oxidative phosphorylation. J Appl Physiol Respir Environ Exerc Physiol. 1981; 51:438–446. [PubMed: 7263450]

60. Moore SJ, Ho IK, Hume AS. Severe hypoxia produced by concomitant intoxication with sublethal doses of carbon monoxide and cyanide. Toxicol Appl Pharmacol. 1991; 109:412–420. [PubMed: 1853342]

61. Halestrap AP. Monocarboxylic acid transport. Compr Physiol. 2013; 3:1611–1643. [PubMed: 24265240]

62. Schwarzkopf TM, Horn T, Lang D, Klein J. Blood gases and energy metabolites in mouse blood before and after cerebral ischemia: the effects of anesthetics. Exp Biol Med (Maywood). 2013; 238:84–89. [PubMed: 23479767]

63. Rosdahl H, Ungerstedt U, Jorfeldt L, Henriksson J. Interstitial glucose and lactate balance in human skeletal muscle and adipose tissue studied by microdialysis. J Physiol. 1993; 471:637–657. [PubMed: 8120827]

64. Balbir A, et al. A search for genes that may confer divergent morphology and function in the carotid body between two strains of mice. Am J Physiol Lung Cell Mol Physiol. 2007; 292:L704–L715. [PubMed: 17098806]

65. Yokoyama T, Misuzu YY, Yamamoto Y. Immunohistochemical localization of tryptophan hydroxylase and serotonin transporter in the carotid body of the rat. Histochem Cell Biol. 2013; 140:147–155. [PubMed: 23266900]

66. Izal-Azcarate A, et al. Immunohistochemical characterization of the rat carotid body. Respir Physiol Neurobiol. 2008; 161:95–99. [PubMed: 18280799]
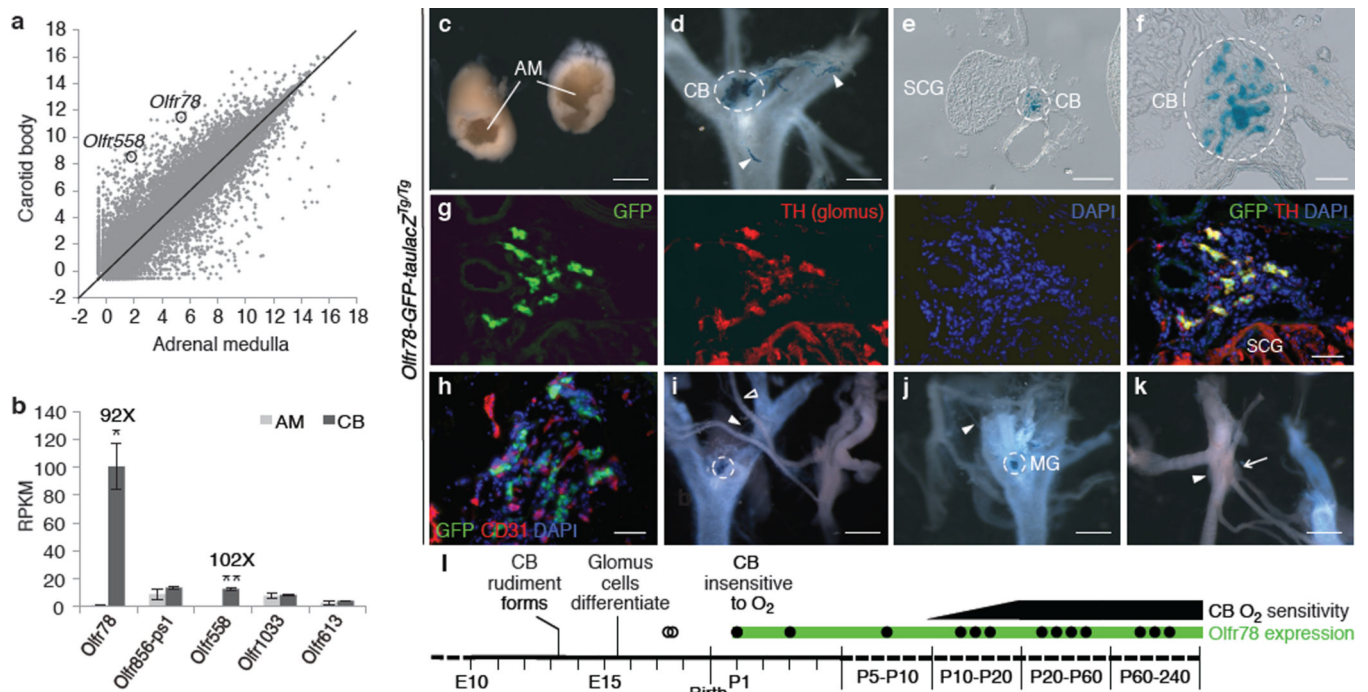
Figure 1. *Olfr78* is expressed in carotid body glomus cells
a, Expression of 26,728 genes in adult mouse carotid body (CB) and adrenal medulla (AM) by RNA sequencing. Log_2 values of number of aligned reads per 10^7 aligned reads generated. **b**, OR genes highly expressed in CB and/or AM. X, fold enrichment (CB/AM). **a, b**, n=3 cohorts of 10 animals each. Data as mean (**a**) or mean ± standard error of the mean (s.e.m., **b**). *P<0.05, **P<0.01 by paired t test by cohort. **c-l**, Expression of *Olfr78* knock-in reporter mouse[11]. **c-f**, X-gal staining (blue) detects taulacZ (β-galactosidase) reporter activity. **c**, Adrenal gland showing adrenal medulla (AM). Reporter not expressed. **d**, Carotid bifurcation (dorsal view, superior cervical ganglion (SCG) removed). Reporter expressed in CB (dashed circle) and sporadic blood vessels (arrowhead). **e, f**, Transverse section of carotid bifurcation (**e**) and close-up (**f**). **g, h**, Immunostaining of CB sections. *Olfr78* reporter expression (GFP; green) co-localized with CB glomus cell marker (tyrosine hydroxylase, TH; red; **g**) but not endothelial cell marker (CD31; red; **h**). TH is also expressed in nerve fibers and SCG. DAPI (blue), nuclei. **i-k**, X-gal stained carotid bifurcations (ventral view). **i**, CB (dashed circle) innervated by carotid sinus nerve (filled arrowhead), a branch of glossopharyngeal nerve (open arrowhead). **j**, "Miniglomerulus" (MG; dashed circle) innervated by glossopharyngeal nerve (arrowhead). **k**, Petrosal ganglion (arrow), nodose/jugular ganglia (arrowhead). Reporter not expressed. **l**, *Olfr78* reporter expression (X-gal staining) during CB development. Filled circles, robust expression; open circles, not detected. Bars, 500 μm (**c-e, i-k**) and 100 μm (**f-h**).
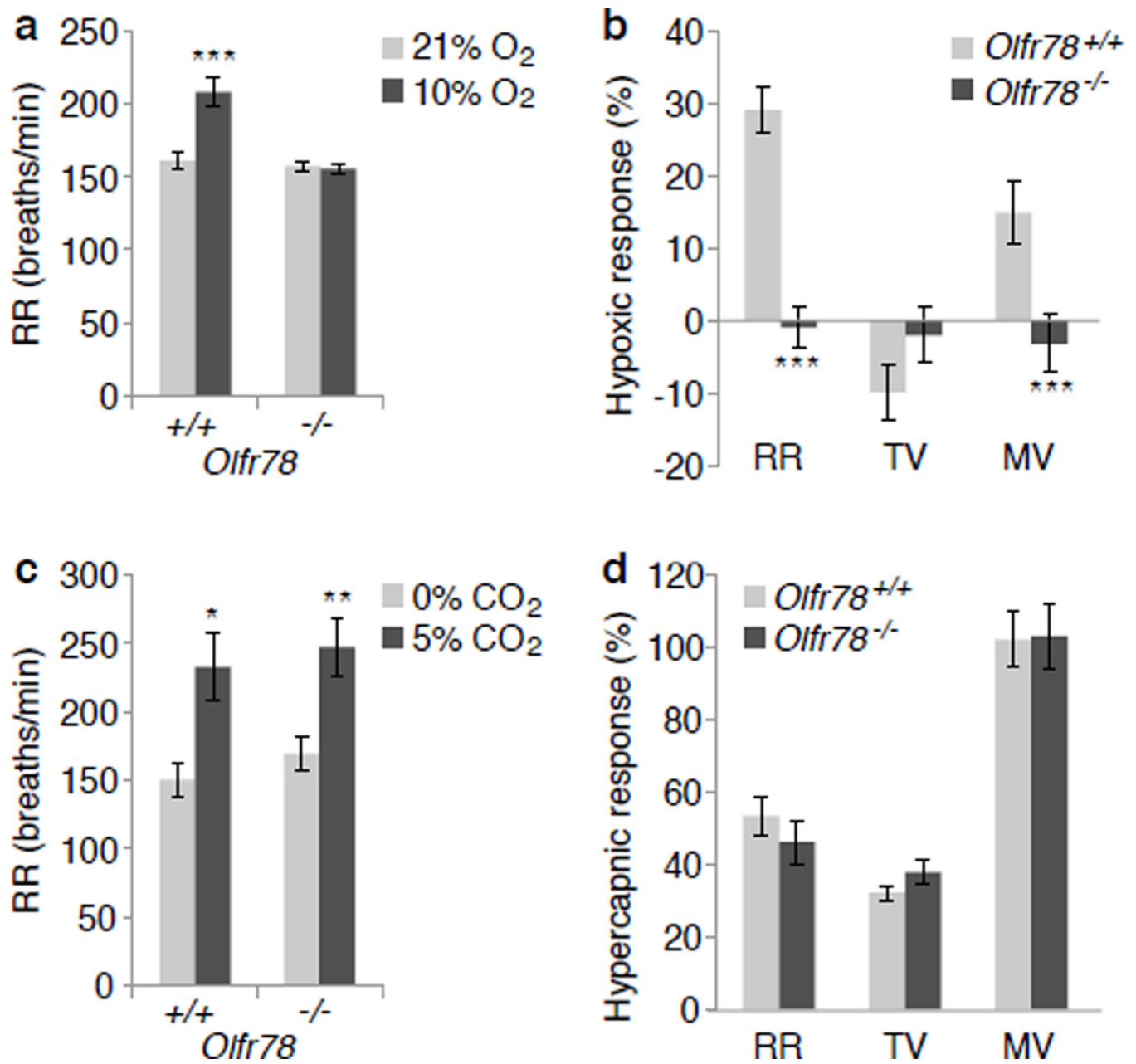
Figure 2. Ventilatory responses of *Olfr78* null mutants to hypoxia and hypercapnia

Respiratory rate (RR), tidal volume (TV), and minute ventilation (MV=RR*TV) by whole body plethysmography of unrestrained, unanesthetized *Olfr78*^{+/+} and *Olfr78*^{−/−} littermates exposed to hypoxia (**a, b**) or hypercapnia (**c, d**). **a, b**, Respiratory rate in hypoxia (**a**) and hypoxic response (**b**) as percent change in hypoxia (10% O_2) versus control (21% O_2). $n=9$ (+/+), 8 (−/−) animals. **c, d**, Respiratory rate in hypercapnia (**c**) and hypercapnic response (**d**) as percent change in hypercapnia (5% CO_2) versus control (0% CO_2). $n=4$ (+/+), 5 (−/−) animals. Data as mean ± s.e.m. *$P<0.05$, **$P<0.01$, ***$P<0.001$ by paired t test (**a, c**) or unpaired t test (**b, d**).
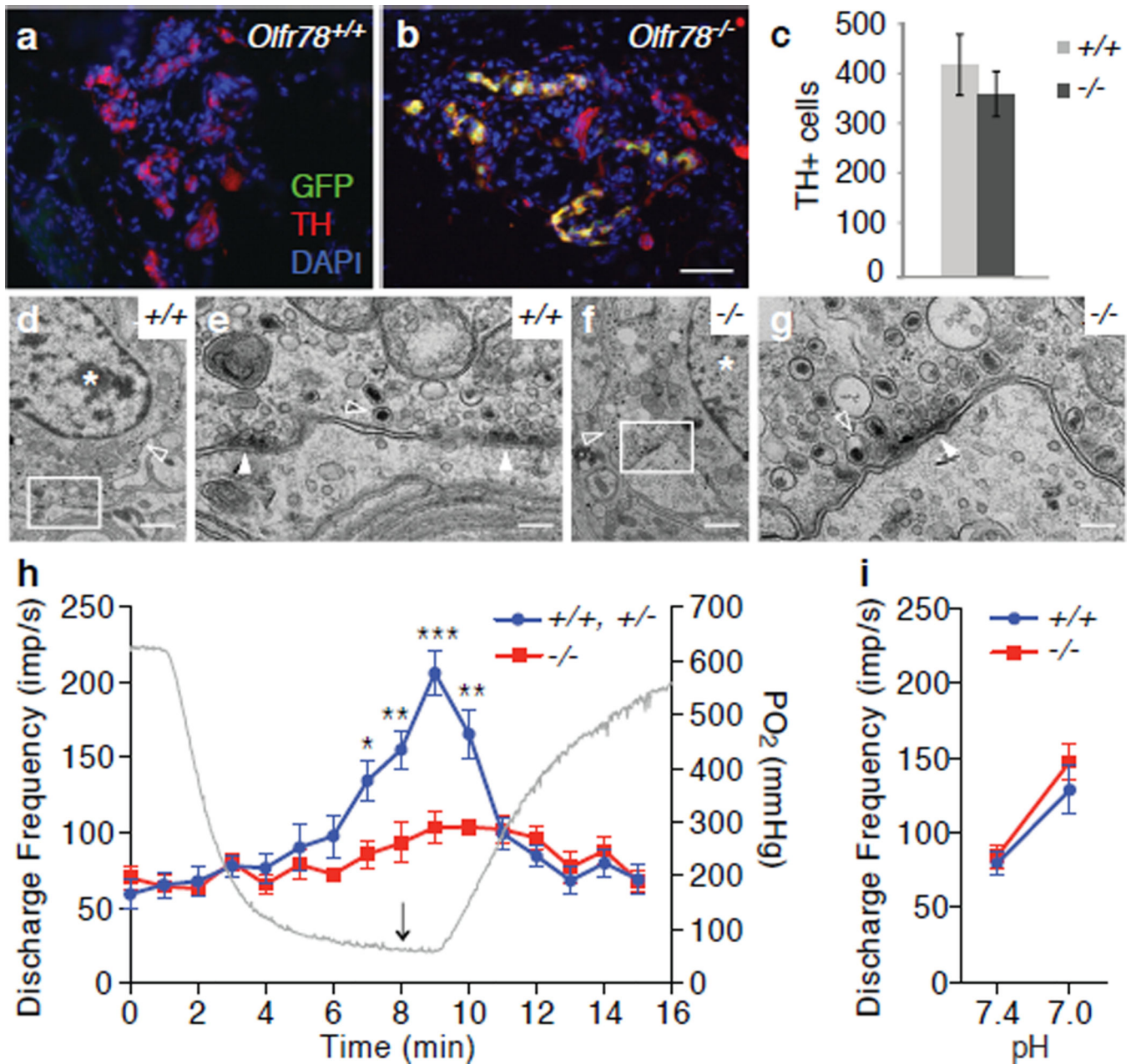
Figure 3. Olfr78 mediates carotid body oxygen sensing

a, b, CB sections from $Olfr78^{+/+}$ control (**a**) and $Olfr78^{-/-}$ knockout allele (**b**) in which *GFP-IRES-taulacZ* replaces *Olfr78* coding region[16]. GFP (green), tyrosine hydroxylase (TH; red), and DAPI (blue). Mutant CB shows normal organization. **c**, Quantification of CB TH-positive cells. $n=8$ (+/+), 14 (−/−) CBs. Data as mean ± s.e.m. $P=0.454$ by unpaired t test. **d-g**, Transmission electron micrographs of $Olfr78^{+/+}$ (**d, e**) and $Olfr78^{-/-}$ (**f, g**) CBs. **e,g**, close-ups of boxed regions. Both wild type and mutant glomus cells have large nuclei (asterisks), large dense core vesicles (open arrowheads), and small clear core vesicles (filled arrowheads). Bars, 100 µm (**a, b**), 600 nm (**d, f**), and 200 nm (**e, g**). **h, i**, CB responses to hypoxia (**h**) and low pH (**i**) assayed by carotid sinus nerve discharge frequency (impulses/

sec) of *Olfr78$^{+/+}$* and *Olfr78$^{+/-}$* controls (blue) and *Olfr78$^{-/-}$* mutants (red). **h**, Hypoxia response as superperfusate changed from bubbling 95% O_2/5% CO_2 to 95% N_2/5% CO_2 (t=0 min) and back to 95% O_2/5% CO_2 (t=8 min, arrow). Gray line, representative time course of PO_2 in recording chamber. Discharge frequency of control nerves began increasing at PO_2=80 mmHg (t=6 min) and peaked at PO_2=60 mmHg (t=9 min). *n*=6 (3 +/+, 3 +/−), 5 (−/−) animals. **i**, Shift from pH 7.4 to pH 7.0. *n*=5 (+/+), 5 (−/−) animals. Data as mean ± s.e.m. *P<0.05, **P<0.01, ***P<0.001 by unpaired *t* test.
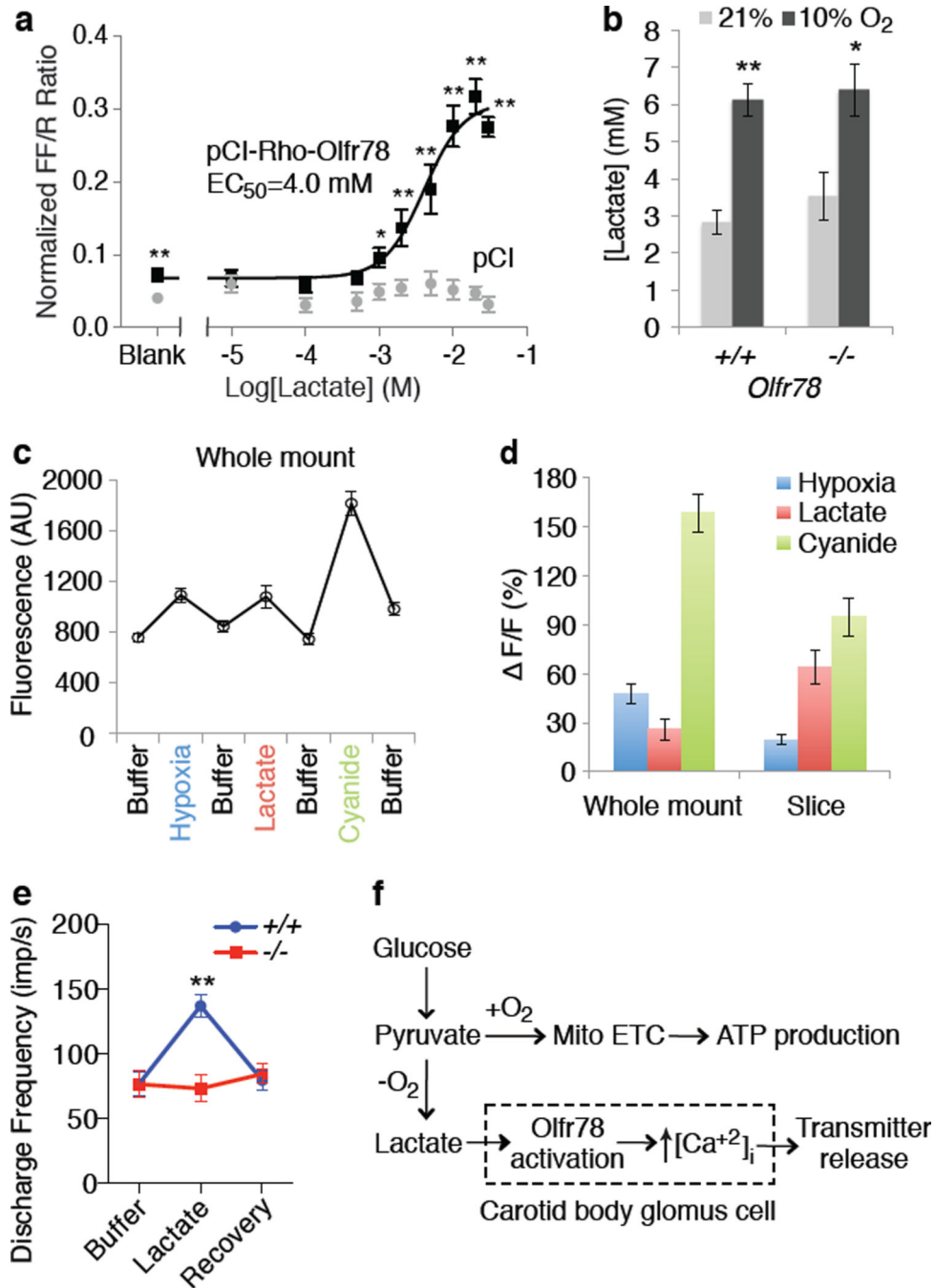
Figure 4. Lactate activates Olfr78 and carotid body sensory activity

a, Lactate activation of Olfr78 expressed in HEK293T cells detected by dual reporter assay (see Methods). Cells transfected with pCI (empty vector, gray) or pCI-Rho-Olfr78 (epitope-tagged Olfr78, black). $n=12$ (4 transfected wells per plate on 3 plates performed on separate days). ANOVA for pCI data, $P=0.478$. **b**, Arterial blood lactate of anesthetized $Olfr78^{+/+}$ and $Olfr78^{-/-}$ littermates exposed to hypoxia for 3 min. $n=4$ (+/+, 21% O_2), 4 (+/+, 10% O_2), 4 (−/−, 21% O_2), 6 (−/−, 10% O_2) animals. **c, d**, Calcium response of GCaMP3-expressing glomus cells exposed to hypoxia ($PO_2=40$–50 mmHg), lactate (30 mM), and

cyanide (2 mM), in whole mount and slice. **c**, Time course of stimuli. Every data point differs from previous point ($P<0.001$ by paired t test). **d**, GCaMP3 fluorescence change (F_1-F_0)/F_0 in percent. $n=42$ (whole mount, all stimuli), 29 (slice, hypoxia and cyanide), 22 (slice, lactate) cells. All changes differ from pre-stimulus ($P<0.001$ by paired t test). **e**, *Olfr78*$^{+/+}$ and *Olfr78*$^{-/-}$ CB response to 30 mM lactate for 10 min, assayed by carotid sinus nerve activity. $n=5$ (+/+), 5 (−/−) animals. **a-e**, Data as mean ± s.e.m. *$P<0.05$, **$P<0.01$ by unpaired t test. **f**, Model of oxygen sensing by Olfr78. In normoxia, pyruvate is efficiently used in Krebs cycle, supplying electrons to mitochondrial electron transport chain (ETC) to produce ATP. In hypoxia, lack of oxygen as final electron acceptor slows ETC, causing pyruvate to accumulate. Pyruvate is converted to lactate, which is secreted and binds Olfr78 on CB glomus cells, increasing intracellular calcium and transmitter release to afferent nerves to stimulate breathing.

Extended Data Table 1

Top 150 genes highly expressed in carotid body vs. adrenal medulla by RNA-seq.

Gene Name	CB*	AM*	CB/AM†	Comment	Gene Name	CB*	AM*	CB/AM†	Comment
Cpne4	9.9	0.4	9.4	Ca^{+2}-dep membrane binding	Cpa3	9.4	3.7	5.7	Peptidase, mast cell
Slc9a2	9.2	0.3	8.9	Na$^+$/K$^+$ exchanger	Dlx6	5.7	0.0	5.7	Hox TF, brain
Coch	10.1	1.2	8.9	Expressed in ear cells	2210407C18Rik	5.2	-0.6	5.7	
Abcc2	9.0	0.6	8.4	ABC transporter	Cwh43	7.0	1.3	5.7	GPI-anchor lipid remodeling
Barx1	7.7	-0.6	8.3	Hox TF, neural crest	Cma1	9.8	4.2	5.7	Chymase, mast cell
Higd1c	11.3	3.2	8.1	Membrane protein	Nmu	5.0	-0.6	5.6	Neuropeptide, neuromedin U
Hmx3	7.3	-0.6	7.8	Hox TF, ear and neurons	Drd1a	5.8	0.3	5.5	GPCR, dopamine receptor 1a
Hmx2	7.6	-0.2	7.8	Hox TF, ear	Sfrp4	9.8	4.3	5.5	Secreted frizzled
Ccl21a	8.2	0.4	7.8	Chemokine	Bcl11b	8.6	3.1	5.5	Tumor suppressor
AB099516	13.4	5.6	7.8	Methyltransferase-like	Myh11	10.6	5.1	5.5	Smooth muscle myosin
Pcolce2	11.3	3.6	7.6	Procollagen peptidase enhancer	Ptx4	4.9	-0.6	5.5	Multifunctional conserved
Lypd2	8.3	0.7	7.5	LY6/PLAUR domain containing	Rxrg	8.7	3.3	5.5	Retinoid X receptor, nuclear
Gkn3	8.7	1.3	7.3	Pseudogene	Pax8	4.9	-0.6	5.5	Paired box TF, thyroid
Mcpt4	8.8	1.4	7.3	Mast cell proliferation	Crhr1	5.7	0.3	5.4	GPCR, hormone
Gm21541	7.3	0.0	7.3	Chemokine	Gm694	4.9	-0.6	5.4	
Ccl21b	7.3	0.0	7.3	Chemokine	Mc4r	7.5	2.1	5.4	GPCR, melanocortin receptor
Gm13304	7.4	0.1	7.3	Chemokine	Sgca	5.3	0.0	5.4	Extracellular matrix
Tpsb2	7.8	0.6	7.1	Tryptase, mast cell	Gm9885	5.4	0.1	5.3	
Cpne5	8.1	1.0	7.1	Ca^{+2}-dep membrane binding	Kcna1	12.4	7.1	5.3	Voltage-gated K$^-$ channel, K$_v$ 1.1
H19	8.7	1.7	7.1	Maternal imprinted	Smim5	8.0	2.7	5.3	Integral membrane protein
Gm10768	7.1	0.1	7.0		Ccl11	9.0	3.8	5.3	Chemokine
Gm1987	8.2	1.3	6.9	Chemokine	Pllp	6.6	1.3	5.2	Involved in myelination
LOC100041504	7.2	0.3	6.9	Chemokine	Galnt9	8.8	3.6	5.2	GalNac transferase
Cst12	6.6	-0.2	6.9	Cysteine endopeptidase	C1qtnf9	6.9	1.7	5.2	Adipokine
Vit	9.3	2.4	6.9	Extracellular matrix	Hcn1	6.6	1.4	5.2	Hyperpol, CNG K$^+$ channel
Mpz	9.0	2.1	6.8	Myelin	Prss12	6.8	1.6	5.2	Trypsin, neuronal plasticity
Ccl21c	7.2	0.4	6.8	Chemokine	Rergl	6.1	0.9	5.2	Putative GTPase
Prdm6	6.3	-0.6	6.8	Histone methyltransferase	4931429I11Rik	6.3	1.1	5.2	

Author Manuscript

Author Manuscript

Author Manuscript

Author Manuscript

Gene Name	CB*	AM*	CB/AM†	Comment
Susd5	8.1	1.3	6.8	Sushi domain containing
Rxfp1	6.6	-0.2	6.8	GPCR, relaxin receptor
Cytl1	10.1	3.3	6.8	Cytokine-like
Olfr558	8.5	1.8	6.8	GPCR, olfactory receptor
Ly6h	11.1	4.4	6.8	Lymphocyte antigen complex
Gpr139	6.2	-0.6	6.7	GPCR
C530044C16Rik	7.7	1.0	6.7	
Olfr78	11.7	5.1	6.7	GPCR, olfactory receptor
Sfrp2	10.3	3.6	6.6	Secreted frizzled-related
Pln	9.4	2.7	6.6	Ca⁺²-ATPase inhibitor, heart
Tph1	7.4	0.7	6.6	Serotonin biosynthesis
Gm10591	7.3	0.6	6.6	Chemokine
Cntnap4	6.0	-0.6	6.5	Neural cell adhesion
LOC100041593	7.3	0.8	6.5	
Thbs4	7.3	0.8	6.5	Cell adhesion glycoprotein
Tnmd	6.3	-0.2	6.5	Cartilage-specific glycoprotein
Gpr20	7.1	0.6	6.5	GPCR
Cntn5	5.9	-0.6	6.5	Neural cell adhesion
Dgkh	11.2	4.8	6.4	Diacylglycerol kinase
Xirp1	5.9	-0.6	6.4	Actin binding
Ptx3	7.1	0.8	6.4	Innate immunity, inflammation
Prom1	9.1	2.7	6.4	Adult stem cell maintenance
Nov	9.2	2.8	6.4	Extracellular matrix, cancer
Adamtsl3	6.9	0.6	6.3	Metalloprotease, cancer
Gdnf	7.1	0.7	6.3	Glial derived neurotrophic factor
Dlx5	7.5	1.3	6.3	Hox TF, bone
Inmt	11.8	5.7	6.2	Indolethylamine N-methylase
Mfap5	11.5	5.4	6.1	Microfibril-associated glycoprotein
Scara3	9.4	3.3	6.1	ROS scavenger
Pgf	10.0	3.9	6.0	Placental growth factor
Mustn1	10.0	4.0	6.0	Expressed in muscle and bone
Enpp3	6.8	1.6	5.2	Nucleotide ectoenzyme
Saa1	5.3	0.1	5.2	Serum amyloid
Itgb4	9.3	4.2	5.1	Integrin
Cpn1	4.5	-0.6	5.1	Carboxypeptidase
Cspg4	9.6	4.6	5.0	Extracellular matrix proteoglycan
9130206I24Rik	7.2	2.2	5.0	GPCR
Areg	4.4	-0.6	5.0	EGF/TGF-α homolog, glia
Trabd2b	8.9	3.9	5.0	Neg regulator of Wnt signaling
Chrdl1	9.1	4.2	5.0	BMP4 antagonist, neuron
Ltbp2	7.3	2.4	5.0	Extracellular matrix
Rbp7	7.0	2.1	4.9	Retinol binding protein
Mmm1	7.9	3.0	4.9	Carrier of platelet proteins
Hrk	8.0	3.1	4.9	Promotes apoptosis
Ptgfr	6.8	1.9	4.9	GPCR, prostaglandin receptor
Tpsab1	5.0	0.1	4.9	Tryptase
Pthlh	7.7	2.9	4.9	Parathyroid hormone-like
Fndc1	8.9	4.0	4.9	Fibronectin domain containing
Bmx	6.6	1.8	4.8	Non-receptor tyrosine kinase
Car12	8.7	3.9	4.8	Carbonic anydrase, extracellular
Atp8b1	7.0	2.2	4.8	Cation transport ATPase
Cd163l1	4.6	-0.2	4.8	Scavenger receptor, immune
Gcsam	5.4	0.6	4.8	PDZ domain containing
Acta2	13.9	9.1	4.8	Smooth muscle actin, aorta
Dcn	15.1	10.3	4.8	Extracellular matrix proteoglycan
Dlx6as1	7.2	2.4	4.8	Noncoding RNA, GABA neurons
Chp2	6.9	2.2	4.7	Ca⁺²-binding, pH control
Gm10808	5.2	0.4	4.7	
Col8a1	10.1	5.4	4.7	Collagen
Foxd1	6.0	1.3	4.7	Forkhead TF
Igfbp4	13.2	8.5	4.7	Insulin-like growth factor binding
Alpl	8.5	3.8	4.7	Alkaline phosphatase

Gene Name	CB*	AM*	CB/AM†	Comment
Pkib	12.5	6.5	6.0	cAMP-dep kinase inhibitor
Comp	6.6	0.6	6.0	Cartilage matrix
Gap43	12.3	6.3	6.0	Neuronal growth cone
Shisa3	8.7	2.7	6.0	Fgf and Wnt signaling interactor
Cma2	5.4	−0.6	6.0	Chymase, mast cell
Gjb5	6.1	0.1	6.0	Gap junction
Meox2	9.1	3.2	5.9	Hox TF, mesenchyme
Ptch1	5.7	−0.2	5.9	Phospholipase
Tlx1	5.3	−0.6	5.9	Hox TF-spleen, neurons, T cells
Igfbp6	12.1	6.3	5.8	Insulin-binding protein
Rgs5	14.9	9.0	5.8	GTPase activator
Edn1	8.0	2.2	5.8	Endothelin 1, vasoconstrictor
Rspo1	10.1	4.2	5.8	Activator of Wnt signaling
Upb1	7.0	1.2	5.8	Pyrimidine degradation
Scnn1b	9.4	3.6	5.8	ENaC Na$^+$ channel, beta subunit
Fgf7	6.6	0.8	5.8	Fibroblast growth factor
Dhrs2	6.2	1.5	4.7	Dehydrogenase/reductase
Lmod3	4.5	−0.2	4.7	Expressed in muscle
Rnase1	5.1	0.4	4.7	Secretory RNase
Gm15998	4.4	−0.2	4.7	
Cnn1	7.4	2.7	4.7	Thin filament associated, muscle
Col2a1	4.1	−0.6	4.7	Collagen
Osr1	8.2	3.6	4.7	TF, odd-skipped related
Hepacam2	6.0	1.3	4.6	Centrosome maturation
Fcer1a	5.1	0.5	4.6	IgE receptor, Fc
Pax9	4.1	−0.6	4.6	Paired box TF
Ncmap	7.5	2.8	4.6	Myelin-associated
Pls1	5.5	0.8	4.6	Plastins, hematopoietic cells
Fbln7	11.1	6.5	4.6	Extracellular matrix adhesion
Folr2	8.4	3.8	4.6	Folate receptor
Msx1	6.9	2.3	4.6	Hox, craniofacial
Tmem158	12.7	8.1	4.6	Peptide receptor

*
CB and AM values are log2(aligned reads per 10^7 reads) as Fig. 1a.

†
Log2(CB/AM) ratios as in Extended Data Fig. 2a. All genes were significantly different between CB and AM by paired t test ($P<0.05$), except Bmx ($P=0.056$). Yellow highlight, genes for olfactory receptors. Blue highlight, genes previously shown to be expressed in CB (ref[40,65,66]). TF, transcription factor; GPCR, G protein-coupled receptor; ROS, reactive oxygen species; CNG, cyclic nucleotide-gated.